

博士論文

Structural and Functional Analysis of  
Kinesin Superfamily Protein KIF19A

(キネシンスーパーファミリータンパク質  
KIF19Aの構造および機能の解析)

王 斗斗  
Wang Doudou

# Contents

<b>Abstract.....</b>	<b>1</b>
<b>Introduction.....</b>	<b>3</b>
<b>Materials and Methods.....</b>	<b>9</b>
<b>Results.....</b>	<b>18</b>
<b>Discussions.....</b>	<b>34</b>
<b>Figure Legends.....</b>	<b>41</b>
<b>Figures.....</b>	<b>49</b>
<b>Tables.....</b>	<b>62</b>
<b>References.....</b>	<b>65</b>
<b>Acknowledgements.....</b>	<b>69</b>

## Abstract

KIF19A was reported as a unique dual functional motor, which can actively walk along the microtubule (MT) to target its plus end, where KIF19A can depolymerize the MT and regulate MT dynamics. In this study, to elucidate the molecular mechanism of the walk and depolymerize functions, here, I determined the crystal structure of the mouse KIF19A motor domain in the complex with ADP and also examined the ATPase activities, the MT-based motilities and MT depolymerization abilities of the KIF19A wild type motor domain and the mutants. In comparison with the previously solved motor domains of the various KIFs, remarkable features of KIF19A motor domain are clustered on its MT-binding side: the disordered helix  $\alpha 4$ , the short helix  $\alpha 6$ , the long and wide loop L2, and the flexible Loop L8. My data indicate the functional anatomy for the dual function of KIF19A. Basic amino acids cluster of the loop L2 of KIF19A enables it to be tethered to MTs by the flexible ionic interaction with the E-hook of tubulins so that KIF19A processively walks along the MT-lattice. I suppose, when KIF19A reaches the plus-end of the MTs, the specific asparagine residue 297 in  $\alpha 5$  of KIF19A that increases the flexibility of MT-binding interface  $\alpha 4$ , as well as the flexible loop L8 facilitates the binding to the curved

protofilament and then, the tubulin dimer is removed from the plus end of MTs by using the energy generated from ATP hydrolysis.

## Introduction

Kinesin superfamily proteins (KIFs) are mostly molecular motor proteins, which move along microtubules. KIFs hydrolyze the ATP to provide the energy to support various cellular functions such as intracellular transport and MT dynamics regulation (Miki et al. 2005; Hirokawa et al. 2009). In the standardized nomenclature, KIFs are classified into 14 families (Figure 1), from Kinesin-1 to Kinesin-14, and share a highly conserved motor domain sequence. Kinesin-1 to Kinesin-12, namely N-kinesins, have the motor domain in their N-terminus, Kinesin-13, namely M-kinesins, in the middle, and Kinesin-14, namely C-kinesins, in their C-terminus (Lawrence 2004). A highly conserved motor domain that contains both the MT- and ATP- binding sequences is a minimal functional domain to catalyze ATP and produces the MT-based motility toward the plus-end in N-kinesins and toward the minus-end in C-kinesins. In M-kinesins (Kinesin-13), the motor domain acquired the MT-depolymerizing activity at the sacrifice of the active transport along the MT.

KIF19A belongs to a unique Kinesin-8 family, which has both the N-kinesins and

M-kinesins characteristics. Kinesin-8s utilize the energy from hydrolyzing ATP to walk toward the MT plus-end like the members in N-kinesins, and depolymerize the MT to regulate the MT dynamics like the members in M-kinesins (Niwa et al. 2012).

The motor domain alone of M-kinesin, Kinesin-13, can depolymerize the MT albeit the class-conserved neck at its N-terminal side increases the activity significantly (Maney 2001; Ogawa et al. 2004; Hertzner et al. 2006). M-kinesins adjust the surface shape suitable for the tubulin subunits with curved conformation so that M-kinesins can induce a depolymerizing curved conformation of the tubulin subunits at the MT ends to depolymerize the MT (Desai et al. 1999). On the contrary, M-kinesins do not fit to the tubulin straight protofilament conformation subunits, which are found at the MT lattice. To target both ends of the MTs, Kinesin-13s diffuse freely along the MT lattice (Helenius et al. 2006) and utilize the MT end-stimulated ATPase activity to release the isolated tubulin dimers (Hunter et al. 2003).

The crystal structure of two Kinesin-13 catalytic domains revealed its characteristic interface suitable for binding to the curved tubulin subunits rather than their straight conformation (Ogawa et al. 2004; Shipley et al. 2004). Albeit the fact that the overall structure of the motor domain is very similar with other N-kinesins or C-kinesins,

Kinesin-13 has the long loop L2 and the loop L8 that project toward the MT/tubulin. These characteristic conformations of two loops enable Kinesin-13 to fit perfectly to the curved tubulin interface, thus depolymerize the MT. At the tip of the loop L2, the class-specific lysine-valine-aspartate (KVD) motif is found, which is necessary for the effective depolymerase activity, and the mutagenesis and deletion analysis of KVD motif supports the structural implications (Ogawa et al. 2004; Shipley et al. 2004).

Kinesin-8s share the highly conserved motor domain with plus-end directed motor N-kinesins, albeit most extensively-studied Kinesin-8, Kip3p (budding yeast Kinesin-8; homologue of mammalian KIF18), was reported to require its C-terminal tail as one of its MT-binding site to prevent its detachment from the MT lattice (Mayr et al. 2011; Stumpff et al. 2011; Su et al. 2011; Weaver et al. 2011). With the assistance of the C-terminal tail, the Kip3p is highly processive ( $>5\mu\text{m}$ ) and the processivity facilitates the long MT to accumulate the increasing motor concentration, which contributes to explain Kinesin-8s depolymerize long MTs more effectively than short ones (Varga et al. 2006). The Kip3p was also reported to depolymerize MT by removing the tubulin dimers from the plus end (Gupta et al. 2006; Varga et al. 2006). Multiple Kip3p acts cooperatively to mediate

length-dependent MT depolymerization and one possible model for a length-dependent manner is the incoming Kip3p bump off the pausing motor at the MT plus end (Varga et al. 2009).

The structural studies of human Kinesin-8 motor domain KIF18A provided some clues indicating the molecular mechanism of the dual functional Kinesin-8 motor domain (Peters et al. 2010). KIF18A possesses an unusual extended loop L2. Since the loop L2 is known to be responsible for the MT-depolymerizing activity of Kinesin-13, this long L2 was thought to be also necessary for the MT-depolymerizing activity of Kinesin-8. However, this long loop L2 was missing in the crystal structure of KIF18A because of its flexibility. Furthermore, the rigid KVD finger like motif of Kinesin-13, which is essential for the MT depolymerization, is lacking in the loop L2 of KIF18A. The cryo-EM structure of KIF18A motor domain bound with MT revealed that the disordered loop L2 in the crystal structure formed well-ordered contacts with the MTs surface, albeit the molecular mechanism of the dual-function of Kinesin-8 is still unraveled.

Most of the Kinsin-8 motors play critical roles during the cell division process, such as spindle length regulation (Weaver et al. 2011; Su et al. 2013), mitotic chromosome

alignment control (Kline-Smith & Walczak 2004; Stumpff et al. 2008). Recently, another member of Kinesin-8 motor, KIF19A was reported as a MT-depolymerizing kinesin for ciliary length control (Niwa et al. 2012). *Kif19A*<sup>-/-</sup> mice displayed hydrocephalus and female infertility phenotypes due to abnormally elongated cilia that cannot generate proper fluid flow. In vitro, KIF19A is not only a plus-end-directed motor, but also depolymerize the MTs mainly from their plus ends, which may contribute to regulate the optimal length of motile cilia in mice. KIF19A, therefore, is also the dual functional motor like the Kip3p or KIF18A. From the amino-acid sequence alignment, indeed, KIF19A also has the long loop L2, albeit the amino-acid sequence of L2 is very different between KIF18A and KIF19A. KIF18A has many basic residues in the loop L12, whereas KIF19A does not. Hence, to date, the structural mechanisms of the dual functions of Kinesin-8, either common or distinct between KIF18A and KIF19A, remain elusive.

To elucidate the molecular mechanism of the dual functions, the MT-based motility and depolymerizing MTs, of Kinesin-8, KIF19A, here I determined the crystal structure of the mouse KIF19A motor domain in the complex with the ADP. I also examined the ATPase activities, the MT-based motilities, and MT depolymerization abilities with the wild type

motor domain and the mutants, which were based on the structural observation and sequence alignment with other kinesins. Our data indicated that four key structural elements of the KIF19A motor domain, L2, L8,  $\alpha 4$ - $\alpha 5$  and  $\alpha 6$  might account for its dual functions. Although these four elements are not conserved between KIF19A and KIF18A or between KIF19A and Kinesin-13s such as KIF2C/MCAK, the binding interface for the MT is varied by the contribution of two loops, L2 and L8, resembles with that of Kinesin-13s. The specific feature of KIF19A or Kinesin-8 is that its interface is adaptable both for the straight form of the tubulin-dimer at the MT lattice and its curved form at the MT-end, which enables it to acquire the dual functions.

## Materials and Methods

### Construction and Mutation

The coding region of KIF19A motor domain (residues 1-353) was PCR amplified from pEGFP-N1-KIF19AFL, which contained a full length KIF19A coding sequence and was originally constructed by Dr. Minato (A member of Hirokawa Lab). The forward primer was designed to add the restriction endonuclease site EcoRI, the reverse primer was with an additional 7XHis tag and the restriction endonuclease site Sall. The PCR product was digested by EcoRI and Sall (NEB), following the manufacturer's instruction and then cloned into the pET-21b (+) vector (Novagen), which was transformed into *E. coli* BL21 (DE3) host strain (Novagen).

Two steps of PCR site-directed mutagenesis was used to construct the mutants, which were all based on the wide type construct KIF19A353WT.

The information of primers was listed in Table 1.

## **Protein expression and Purification**

KIF19A353WT and the mutants were expressed in *E. coli* strain BL21 (DE3). Protein expression was induced by addition of IPTG to the LB medium until the OD600 reached 0.6.

A final concentration of 0.4 mM IPTG was used for full induction. The bacteria were incubated at 24 °C for 16 hours with vigorously shaking. The cells were harvested by centrifugation at 3500rpm (SX4750 rotor, Beckman Coulter) for 15min at 4°C and resuspended in the cold Lysis Buffer (see Table 2, all the buffer information was listed in Table 2).

French pressure cell press was used to break the bacteria, followed an ultracentrifuge at 35000g (Type 45Ti Rotor, Beckman Coulter) at 2 °C for 30min. The supernatant was carefully separated from the pellet and gently mixed with the HIS-Select Nickel Affinity Gel (SIGMA-ALDRICH) on a rotating mixer for 25 min at 4°C. The gel was washed with 10 column volumes of Wash Buffer. Then, the proteins were eluted with Elution Buffer. Peak fractions were collected and dialyzed against the Dialysis Buffer 1 for 3 hours. The proteins were loaded on the RESOURCE S 1 ml pre-packed column (GE Healthcare). The linear gradient of NaCl was performed to elute the target protein. The eluted protein was

dialyzed against Dialysis Buffer 2 prior to protein concentrate by the Amicon ultra-4 centrifugal filter units (Milipore). BCA Protein Assay Kit (Thermo Scientific) was used to determine the protein concentration. The protein samples were aliquoted in a small volume for immediately use or flash frozen in liquid nitrogen for further use.

### **Protein Crystallization**

Several commercial kits, Crystal Screen 1/ 2 (Hampton Research), Wizard: Classic 1/2/3/4 (Emerald Bio), Morpheus (Molecular Dimensions) were used for initial crystallization screen. By using hanging drop vapor diffusion method, 1  $\mu$ l KIF19A353WT protein sample at 10 mg/ml containing 0.1 mM ADP was mixed with 1  $\mu$ l reservoir buffer and incubated at 20 °C. Crystals are grown in 10% ethylene glycol, 5% PEG8000, 50 mM Tris-Bicine (pH 8.5), 15 mM MgCl<sub>2</sub> and 15 mM CaCl<sub>2</sub>. The optimal condition for single crystal growing was containing 10% ethylene glycol, 2% PEG8000, 50 mM Tris-Bicine (pH 8.5), 9 mM MgCl<sub>2</sub> and 9 mM CaCl<sub>2</sub>.

### **Structure Determination**

X-ray diffraction data at 2.72 Å resolution were collected at BL41XU beam-line (SPring-8), at the wavelength  $\lambda=1.0$  Å. The anomalous diffraction data were collected at BL1A beamline (Photon Factory), at the wavelength  $\lambda=2.7$  Å. HKL2000 program package (Otwinowski & Minor 1997) was used to index, integrate and scale the data. Using Crystallography & NMR System (CNS, Brunger et al. 1998; Brunger 2007), I found molecular replacement solution using KIF18AMD (PDB: 3LRE) as a search model. The model was rebuilt with the program Coot (Emsley & Cowtan 2004) and refined with Refmac5 (Murshudov et al. 2011). UCSF Chimera was used for structure alignment and visualization (Pettersen et al. 2004).

### **MT polymerization**

Tubulin was purified from porcine brains for six cycles of polymerization/depolymerization. Tubulin was clarified with 100k rpm centrifuge for 30min at 2°C in a TLA110 rotor (Beckman Coulter). For Taxol-stabilized MTs, the clarified tubulin was incubated at 37°C for 2 min, and then gently mixed with Taxol to 0.1 µM final concentration. After another 10 min incubation, Taxol was added to the reaction to 1 µM final concentration. Finally, after

another 10 min incubation, the reaction was gently mixed with Taxol to 10  $\mu$ M final concentration and kept incubating up to 2 hours. For GMPCPP-stabilized MT, 3  $\mu$ M tubulin was mixed with 0.5 mM GMPCPP in BRB80, and incubated at 37°C for 2 hours. The MTs were collected by centrifugation through a 20% glycerol cushion at 37°C for 10 min at 25000 rpm using a TLA100A rotor (Beckman Coulter) in an ultracentrifuge (TLX). The MTs were resuspended in PEM or BRB80.

### **ATPase Assay**

The steady state ATPase kinetics of KIF19A353WT and mutants were measured using an EnzCheck phosphate assay kit (Molecular Probes)(Nitta et al. 2008). In the presence of Pi, which catalyzed by Kinesin, the substrate 2-amino-6-mercapto-7-methylpurine riboside (MESG) was converted enzymatically by purine nucleoside phosphorylase (PNP) to ribose 1-phosphate and 2-amino-6-mercapto-7-methylpurine. This process results in a spectrophotometric shift in maximum absorbance to 360 nm for the product. The absorbance at 360 nm was recorded at 25°C every 5 seconds lasting for 300 seconds by using V-630 Bio spectrophotometer (JASCO) since all the components were mixed in PEM

buffer. The ATPase hydrate rate was calculated from the slope of the absorbance increase line, and measured at different concentration of MT or tubulin. Kinetic data were plotted and fitted the Michaelis-Menten model.

### **Tubulin S preparation**

Dilute tubulin to 5 mg/ml in distilled water and add GTP to 1 mM final concentration. After preincubating in a centrifuge tube at 25°C for 5 min, substilisin was added in a weight ratio of 1/100, with further incubation at 25°C for 45 min. Stop the reaction with PMSF to 0.05% final concentration and incubate on ice for 40 min. Centrifuge at 4°C at 110,000 g for 20 min. Collect the supernatant and determine protein concentration by BCA method. Flash freeze in liquid N<sub>2</sub> and store at -80°C or use freshly. Tubulin S was used to polymerize MTs following the protocol mentioned previously.

### **MT Binding Assay**

To investigate the binding affinities between the KIF19A proteins and MTs, 2 μM of purified KIF19A proteins were incubated with increasing amounts of Taxol-MT (0-40 μM)

in PEM buffer at 25°C for 15 min. After 55000 rpm centrifugation at 25°C for 10 min, in a TLA55 rotor (Beckman Coulter). The Separated supernatant and pellet fractions were loaded onto SDS-PAGE, and the band intensities were analyzed by Image J (NIH). The data were fitted to a bimolecular binding equation (Equation 1), where Y is the fraction of bound KIF19A, and X is the concentration of MTs, using nonlinear regression methods.

$$Y = \frac{B_{max} * X}{K_d + X} \quad (\text{Equation 1})$$

### **MT gliding motility assay**

Flow chamber (Figure 11A) was made for the gliding motility assay. The KIF19A353WT and mutants proteins were immobilized on the cover glass by using PentaHis antibody (Qiagen)(Figure 11B). The surface of the cover glass was further coated with casein (Wako Chemical) to prevent nonspecific binding. After washing, 20 µl KIF19A protein solution (0.1 mg/ml) was injected into the flow chamber and washed out after 3 min incubation. Then, the TMR-labeled MTs in PEM buffer was injected and kept binding 3 min and the glass cover glass was turned face down several minutes to reduce the background fluorescence and prevent extra MTs binding during data collection. Finally, the motility

buffer was supplemented with oxygen-scavenger to minimize photobleaching and injected just before observation. The time-lapse observation was performed at 37°C, using the ELYRA P.1 system (Carl Zeiss) in the TIRF mode. The data were collected every five seconds for 10 min.

### **MT Depolymerization assays**

Depolymerization assays were performed using GMPCPP MTs 250 nM KIF19A wild type or mutants were incubated in BRB80, 5 mM ATP or AMPPNP, and 1.5  $\mu$ M GMPCPP MTs respectively. To determine the  $EC_{50}$ , KIF19A was titrated in different concentration of KIF19A (0-5000 nM) with 1.0  $\mu$ M GMPCPP MTs. All reactions were incubated at 25°C for 15 min, and subsequently centrifuged in a TLA55A rotor (Beckman Coulter) at 55000 rpm for 10 min at 25°C. The supernatant was removed from the pellet, and the pellet was resuspended in BRB80 with the same volumes of the supernatant. Equal volumes of supernatant and pellet were electrophoresed on a 10% SDS-PAGE. The gel was stained with Coomassie Brilliant Blue and scanned. The fraction of free tubulin was quantified and analyzed by using ImageJ (NIH). The data were plotted and fitted to the four-parameter

logistic equation (Equation 2) and the  $EC_{50}$  was calculated using KaleidaGraph 4.0 software

(Synergy), where Response is the amount of free tubulin,  $R_{min}$  is the baseline,  $R_{max}$  is the

maximal response, X is the KIF19A concentration, and H is the Hill slope.

$$\text{Response} = \frac{R_{min} + (R_{max} - R_{min})}{1 + 10^{H \cdot \log\left(\frac{EC_{50}}{x}\right)}} \quad (\text{Equation 2})$$

## Results

### **Expression, Purification and Crystallization of the KIF19A motor domain constructs**

#### **KIF19A353WT.**

KIF19A belongs to the Kinesin-8 family, which shares a highly conserved N-terminal motor domain sequence among N-kinesins (from Kinesin-1 to Kinesin-12)(Lawrence 2004).

Kinesin neck linker, which varies from different kinesin families, not only links the motor domain to the dimerization coiled-coil domain, but also has emerged as a crucial structural element in the motility function. In this study, both the motor domain and the following neck linker were included in the construct, KIF19A353WT (residues from 1 to 353, Figure 2A), which was mainly used for crystallographic and other functional research. All the mutant constructs in this study were based on this wild type construct.

The KIF19A353WT was expressed in *E.coli* BL21 (DE3), and purified sequentially by immobilized metal affinity chromatography (IMAC) and cation exchange chromatography (CIEX) (Figure 3A; see Materials and Methods for details). The purity is about 95%, judged

by SDS-PAGE Comassie Brilliant Blue staining gel (Figure 3B) and the yield is approximately 8 mg from 1L *E.coli* culture.

KIF19A353WT and ADP were co-crystallized in the buffer, which used ethylene glycol and PEG8000 as precipitant. Single crystals (Figure 3C) were grown at 20°C using hanging drop vapor diffusion method. X-ray diffraction data at 2.72 Å resolution (Figure 3D) were collected at BL41XU beam-line (SPring8) and then was processed through HKL2000 program package (Otwinowski & Minor 1997).

### **Structure Determination with the Guide of S-SAD.**

The tertiary structure was tried to be solved by using molecular replacement method. During the structure determination process of KIF19A motor domain, however, I found one unusual helical density that was situated close to the loop L2 (Figure 4A). It was difficult to assign the certain amino acid sequence to it because it was not observed in any other kinesin structures. At that time, most residues were fitted into the electron densities with the R-factor = 0.2856 so that the possible candidate sequences corresponding to this helical density were limited to the following two regions, the loop L2 or the helix  $\alpha 4$ . Since the

helix  $\alpha 4$  has one cysteine residue whereas no cysteine or methionine residue is included in the loop L2, we considered combining a sulfur single-wave length anomalous diffraction (S-SAD) (Hendrickson & Teeter 1981; Dauter et al. 1999), which was based on better anomalous signal from protein sulfur atoms obtained at longer X-ray wavelength, to clarify which elements should be assigned to it.

X-ray diffraction data was collected using the wavelength  $\lambda = 2.7 \text{ \AA}$  at the beam line BL1A (Photon Factory). As a consequence, the anomalous diffractions of sulfur atom in Met or Cys residues of the protein as well as the phosphorus atom in ADP were successfully detected. Figures 3B and 3C show the examples of the anomalous signals from the sulfur atom in Met248 (Figure 4B) and phosphorus atoms in ADP (Figure 4C). Around the corresponding helical density, one strong anomalous signal was detected (Figure 4D), indicating that the uncertain helical density was the part of the helix  $\alpha 4$  and the anomalous signal came from the diffractions of the sulfur atom at the Cys283 residue. In this way, I could finally determine the complete tertiary structure of KIF19A motor domain with the R-factor of 24.53%. Data collection and refinement statistics are shown in Table 3.

## **Crystal structure of the KIF19A motor domain constructs KIF19A353WT in ADP**

### **State**

The overall structure of KIF19A motor domain shared a similar triangle-shape structure with other kinesins, which consists of a central  $\beta$ -sheet of eight strands, sandwiched between six  $\alpha$ -helices, three on either side (Sack et al. 1999)(Figure 5). In KIF19A353WT atomic structure,  $Mg^{2+}$ -ADP was found embedded in the nucleotide-binding pocket, which shares remarkable structural homologies with myosins and G-proteins (Vale 2003). The loop L4, known as the “P-loop”, interacts with the phosphate group of the bound nucleotide (ADP). The switch I region, consisted of the C-terminal end of  $\alpha$ 3 and the following loop L9, forms the binding pocket and may undergo the conformational changes to contributes to the ATP hydrolysis. Part of loop L9, called the switch I loop and regarded to sense the  $\gamma$ -phosphate, is disordered in my structure. In comparison with the previously solved motor domains of the various KIFs, remarkable features of KIF19A motor domain seem to be concentrated on its MT-binding side; the disordered helix  $\alpha$ 4, the short helix  $\alpha$ 6, the long and wide loop L2 and the flexible loop L8. The helix  $\alpha$ 4 is included in the switch II structural element that is the main contributor of the MT-based kinesin motility and changes

its conformation during the hydrolysis of ATP. The helix  $\alpha_4$  of KIF19A is atypically distantly positioned from the motor core. The helix  $\alpha_6$  serves as a base for the neck-linker element that is important for both the regulation of the ATPase activity and the MT-based kinesin motility (Case et al. 2000). Its deforming shortness by more than one turn is expected to affect the conformation of the neck-linker. The loop L2 is located at the minus-end side (rear side) of the MT-binding surface of kinesin motor domain and was reported to be necessary for the MT depolymerizing activity of Kinesin-13. The loop L2 of KIF19A is atypically long, comparable to that of Kinesin-13, suggesting the MT depolymerizing activity of KIF19A. Interestingly, the acidic and basic residues are concentrated at its N-terminal and C-terminal sides, respectively, and hydrophobic residues are positioned at the tip of this loop. From the next section, further comparisons of KIF19A motor domain to other motors (KIF18A; KIF2C; KIF4) to clarify the characteristic features of KIF19A motor domain.

### **Structural Features of KIF19A Motor Domain.**

KIF19A was reported to possess the dual function, the MT-based plus-end directed motility

and the MT depolymerizing activity. This feature was also found in KIF18A that belongs to the same subclass Kinesin-8 with KIF19A. I first compare the KIF19A structure with this closest relative KIF18A (Figure 6A, 6B). KIF19A is very similar with KIF18A. Both have the long loop L2 that might be necessary for the MT-depolymerizing activity, albeit the most amino acid residues are missing in the crystal structure of KIF18A. Despite the comparable length of L2 between KIF18A and KIF19A, the amino-acid sequence of L2 between KIF18A and KIF19A is very different (Figure 6C), indicating the distinct functions of these motors. The conformational difference of the helix  $\alpha_6$  should be also noted. The helix  $\alpha_6$  of KIF19A is shorter than that of KIF18A by more than one turn. From the amino acid sequence analysis, KIF19A has the atypical glycine residue close to the C-terminal end of this helix that might destabilize and shorten it (Figure 6D). It is still uncertain why the helix  $\alpha_6$  of KIF19A is shortened and further biochemical study is necessary.

Most remarkable difference between them was found in the switch II helix  $\alpha_4$ . The helix  $\alpha_4$  of KIF18A is typical “ATP-like” conformation that was often observed in the crystal structure of kinesin motor domains (Kikkawa 2008; Peters et al. 2010). However, The helix  $\alpha_4$  of KIF19A is destabilized and distant from the motor core (Figure 5B). By the careful

observation of the amino acid sequence (Figure 6E), I found that the proline residue that is located at the starting point of the helix  $\alpha 5$  and highly conserved in all the kinesin superfamily proteins are replaced by the asparagine residue N297 in KIF19A. Since the proline residue is often found at the starting point or the ending point of the helix and plays a key role to take the stable helical structure, I expected that this mutation should be the key to understand the KIF19A specific function. To confirm this idea, mutational, biochemical, and biophysical assays were performed, as described later.

I next compared the KIF19A structure with the MT depolymerizing motor KIF2C (Figure 7A, 7B), which belongs to the Kinesin-13 family. KIF2C has two specific features on the tubulin-binding surface, the loops L2 and L8, which enables it to fit the curved tubulin interface rather than the straight MT interface (Ogawa et al. 2004). The loop L8 of KIF2C is protruded toward the tubulin/MT, whereas that of KIF19A is not. About the loop L2, KIF2C and KIF19A have comparable length of L2 (Figure 7C). KIF2C has the slender loop L2 that has the KVD finger at its tip (Figure 7D). On the other hand, KIF19A has the long, fan-shaped L2 that has the hydrophobic tip sandwiched by the acidic and basic clusters (Figure 7E). Despite the acidic-hydrophobic-basic order seem to be conserved

between KIF2C and KIF19A, their shape is distinct each other (Figure 7C). All KVD residues of KIF2C are necessary for the MT-depolymerizing activity of KIF2C (Ogawa et al. 2004; Shipley et al. 2004) . To elucidate the functional roles of acidic and basic clusters as well as the hydrophobic tip, I introduced the mutations and performed the biochemical and biophysical studies, which described in the later section.

Finally, the KIF19A structure was compared with the typical plus-end directed motor KIF1A and KIF4. In comparison with the KIF1A-ADP structure (Figure 8A), the conformation of L8- $\alpha$ 3-L9 is considerably different in addition to the switch II helix as well as the loop L2. During the process of structural comparisons, I noticed that the switch I conformation of KIF19A-ADP might resemble the closed information of switch I (Eg5-AMPPNP or KIF4-AMPPNP). Hence I compared it to that of KIF4-AMPPNP (Figure 8B). From this comparison, I found that the L8- $\alpha$ 3-L9 conformation of KIF19A-ADP highly resembles that of KIF4-AMPPNP, albeit the 12° clockwise rotation occurs in KIF19A to open the nucleotide-binding pocket. Tubulin/MT binding to L8 of KIF19A might trigger the counter clockwise rotation of this cluster to close the nucleotide-binding pocket to hydrolyze ATP (Figure 8C).

### **Characterization of KIF19A ATPase.**

As previously reported, KIF19A does not only move very slowly along the MTs ( $21 \pm 3$  nm/sec (Niwa et al. 2012), but also depolymerizes the MTs mainly from their plus-ends.

This character is similar to the neighboring motor Kip3p, which is a well-characterized Kinesin-8 motor, and it is expected that KIF19A ATPase will be mildly activated by both the MTs and tubulins. To confirm this idea, we first examined the steady-state ATPase activity of the wild type construct in the absence/presence of the MTs or tubulins.

The basal ATPase activity of KIF19A motor domain in the absence of MTs or tubulins is comparable to the other kinesin motors including the Kinesin-8 motor Kip3p ( $k_{\text{cat}} = 0.006 \pm 0.0004 \text{ s}^{-1}$ , Figure 9A). Then, its activation by the MTs or free tubulin-dimers was checked. As a result, its ATPase was not only activated  $\sim 200$  times by MTs to reach a maximum rate of  $1.05 \pm 0.03 \text{ s}^{-1}$  ( $k_{\text{cat,WT, MT}}$ , Figure 9B) and but also was activated  $\sim 100$  times by tubulin-dimers to reach a maximum rate of  $0.53 \pm 0.02 \text{ s}^{-1}$  ( $k_{\text{cat,WT, Tub}}$ , Figure 9C). This character is similar with the other Kinesin-8 subfamily proteins and the Kinesin-13 subfamily proteins both of which show the MT depolymerizing activities.

Next, I examined how the several mutations in the loop L2 or the helix  $\alpha 5$ , which takes the characteristic conformation in KIF19A motor domain in comparison with other kinesin motors, affect the ATPase activity of KIF19A. For the helix  $\alpha 5$ , the asparagine residue N297 at the starting point of  $\alpha 5$  was mutated to proline residue (N297P) because the corresponding proline residue is highly conserved among most KIFs. For the loop L2, I divided it into three portions, the negative cluster (E49, D50, D52, D53) and the positive cluster (R56, H58, R59, R61), that were each or both mutated to alanines (NC2A, negative cluster to alanines; PC2A, positive cluster to alanines; AC2A, both to alanines).

Interestingly, N297P mutation causes the opposite effects to the MT- and tubulin-stimulation. The MT-stimulated ATPase activity of N297P mutant exhibited about 30% higher turnover rate than the wild type ( $k_{\text{cat, N297P, MT}} = 1.33 \pm 0.05 \text{ s}^{-1}$ ), on the contrary, the tubulin-stimulated ATPase rate of N297P was only about 0.6 fold of the wild type ( $k_{\text{cat, N297P, Tub}} = 0.32 \pm 0.01 \text{ s}^{-1}$ ). This suggests that KIF19A specific asparagine residue N297 might reflect the adaptation of the KIF19A interface to the curved tubulin-dimer interface to acquire the depolymerizing activity of the MT.

Two kinds of loop L2 mutations also differently affected the KIF19A ATPase.

Comparing to the KIF19A wild type, PC2A showed much lower turnover rate in the presence of MTs ( $k_{\text{cat, PC2A, MT}} = 0.33 \pm 0.01 \text{ s}^{-1}$ ) or tubulins ( $k_{\text{cat, PC2A, Tub}} = 0.09 \pm 0.001 \text{ s}^{-1}$ ). PC2A mutation strongly increased the  $K_{\text{M, MT}}$  (Figure 9E), suggesting that the positive charged residues in L2 strengthens the MT binding at the weak-binding state, like the tethering effect of K-loop of KIF1A to the MT (Okada & Hirokawa 2000). On the other hand, NC2A mutation decreased both the  $K_{\text{M, MT}}$  and  $K_{\text{M, Tub}}$ , albeit the turnover rate was not affected or rather decreased. This indicates that the negative charged residues in L2 rather weaken the tethering effect of KIF19A to the MT. This tuning might positively affect the some function such as the MT depolymerizing activity and further biochemical study is regulated to clarify its functional role. AC2A mutation showed similar effect with the PC2A mutation, suggesting the dominant effect of the PC2A mutation over the NC2A mutation. It should be noted here that when purifying the NC2A and AC2A, they were unstable and easy to be aggregated in the buffer even at low temperature so that the further reliable biochemical and biophysical experiments were difficult to be performed.

### **KIF19A Tethers MTs Using Basic Cluster of L2 of KIF19A and E-hook of Tubulin.**

Based on the results of the ATPase kinetics of KIF19A wild type and mutants, the apparent binding affinity of KIF19A for the MT was expected to be weakened especially by the mutation of the positive cluster of L2 to alanines, PC2A. To confirm it, I examined the MT-binding affinity of wild type and its mutants. Using a MT co-sedimentation assay, we found that KIF19A353WT ( $K_d \sim 0.62 \mu\text{M}$ ) and N297P ( $K_d \sim 0.98 \mu\text{M}$ ) mutant have similar affinity for MTs, as was expected (Figure 10A). On the other hand, PC2A showed more than 10 times lower affinity for MTs than the wild type ( $K_d \sim 9.7 \mu\text{M}$ ). And also as previously reported, Kip3p tubulin-activated ATPase is inhibited by high salt concentration (Gupta, 2006). It is reasonable to speculate the positive charged residues probably interact with some negative charged residues in tubulin.

To address which structural elements of tubulin are responsible for interaction with KIF19A motor domain, I incubated KIF19A with two kinds of MTs, normal tubulin polymers and tubulin-S polymers, in the presence of non-hydrolysable ATP analogue AMPPNP. Tubulin-S which was obtained by limited subtilisin proteolysis of tubulin dimer, lacks the cluster of extensive negative charged residues at the C-terminal tail of  $\alpha$ - and  $\beta$ -tubulins, namely E-hook. Whatever the binding ratio was 1:1 or 1:2.5, much less amount

of KIF19A was seen in the tubulin S assembled MTs pellet (Figure 10B), indicating that E-hook of tubulin is responsible for the KIF19A-MT interaction. Therefore, KIF19A tethers the MTs mainly by the ionic interaction between the basic cluster of the loop L2 and E-hook of tubulins.

### **Asparagine Residue at $\alpha 5$ has a Disadvantage for the Motility.**

Kinesin-8 family members were reported to be a slow plus end-directed motor (Gupta et al. 2006; Mayr et al. 2007; Niwa et al. 2012). To demonstrate the relationship between the KIF19A motility and the Asparagine residue mutation, MT-gliding assays were performed. KIF19A was fixed on the surface of the flow chamber (Figure 11A), and caused the MTs to slide (Figure 11B). Kymographs are used to analyze the trajectories of the moving MTs in a time-resolved manner (Gell et al. 2010). In the representative kymographs (Figure 11C) for MTs moving on wild type and N297P mutant, gliding velocities can be evaluated by the moving distance ( $d/d'$ ) and dwell time ( $t$ ). The MT-gliding velocity of wild type was  $7.71 \pm 2.47$  nm/sec (Figure 11D), which was comparable to the ATPase turn over rate considering that the step size of KIF19A caused by one ATPase cycle is about 8 nm, the

length of one tubulin-dimer. The N297P mutant driven MT-gliding velocities ( $11.01 \pm 1.86$  nm/sec) observed in this study were about 40% faster than that of wild type. The higher motility speed of N297P is consistent with the ATPase activity results. This means that N297P mutation has an advantage for the MT-based motility. That is, along the cause of evolution, KIF19A might have selected the mutation from the proline to the asparagine to obtain the MT depolymerizing activity at the expense of the speed of the MT-based motility.

**Both Asparagine Residue N297 and Loop L2 Contribute to the MT depolymerizing activity.**

I finally examined the MT depolymerization assay to address which region is responsible for the MT depolymerizing activity of KIF19A. I incubated the same amount KIF19A (wild type and mutants) with GMPCPP-stabilized MT in the presence of 5 mM MgATP or non-hydrolysable ATP analogue AMPPNP. 5 mM AMPPNP almost blocked the MT depolymerizing activity of KIF19A wild type. Most KIF19A with AMPPNP remained in the MT pellet, indicating that it was not released from the MT (Figure 12A). Thus, contrast

to the depolymerizing activity of Kinesin-13 KIF2C/MCAK, KIF19A requires the ATP hydrolysis to depolymerize the MT. It is probably because KIF2C can target the both ends of the MT by passive diffusion without the energy from the ATP hydrolysis(Hunter et al. 2003), whereas KIF19A needs plus-end directed active motility to target the MT plus-end. This also explains that KIF2C depolymerizes the MT from both ends, whereas KIF19A depolymerizes it mainly from its plus-end.

N297P and several mutations of L2 more or less decreased the depolymerization activity of KIF19A (Figure 12A). I examined the depolymerizing activity of wild type of KIF19A, N297P, PC2A, and L55A (in the hydrophobic tip of L2) in more detail to determine the effective concentration at which the enzyme gives 50% MT depolymerization activity ( $EC_{50}$ ). For each concentration, the fraction of MTs to free tubulin was quantified and plotted with the log of the KIF19A concentration. For wild type, N297P, and L55A, there was a clear difference of the  $EC_{50}$  between the wild type (KIF19AWT~190 nM) and the mutants (N297P~283 nM, L55A~ 385 nM), which was provided by fitting the data to the dose-response curve, albeit the MTs were almost depolymerized to soluble tubulin at high enzyme concentrations. For PC2A, even at the highest enzyme concentration (5000 nM)

used in this assay achieved approximately 50% depolymerization activity of the wild type (Figure 12B). This right shift of the curve is consistent with the lowest binding affinity of PC2A for the MT. Nevertheless, the mutations to the helix  $\alpha 5$  as well as the loop L2 decreases the MT depolymerizing activity and among them, PC2A mutant showed most severe MT disassemble deficiency.

## Discussions

As a unique class member of kinesin superfamily proteins, Kinesin-8s possess both the MT-based plus-end directed motility and the MT depolymerizing activity (Gupta, 2006, Varga, 2006). To elucidate the molecular mechanisms of the dual functions of Kinesin8, KIF19A, I determined the 2.72 Å resolution crystal structure of the mouse KIF19A motor domain. Based on the structural data, several biochemical and biophysical assays were performed to clarify the functional roles of KIF19A specific structural elements.

### **Specific Structural Elements of KIF19A Motor Domain.**

The overall structure of KIF19A motor domain shares the similar architecture with other kinesins, except for the following four regions, 1) the loop L2, 2) the L8- $\alpha$ 3-L9 (switch I), 3) the L11- $\alpha$ 4-L12- $\alpha$ 5, 4) the helix  $\alpha$ 6, all of them are involved in the MT-binding interface.

About L2 and L11- $\alpha$ 4-L12- $\alpha$ 5, I discussed at the next section based on the mutational, biochemical and biophysical assays. The loop L8 is one of the major MT-binding interfaces

and the L8- $\alpha$ 3-L9 cluster is retracted from the MT/tubulin in the crystal structure. The tip of L8 remains flexible in the absence of the MT/tubulin. This conformation is conserved between Kinesin-8 subfamily (both KIF18A and KIF19A) and might give a flexibility of the interface of Kinesin-8 to adopt both the straight and curved interface of tubulin-dimers. The helix  $\alpha$ 6 takes the unusually shorter form in comparison with the previously solved any structures of KIFs including KIF18A. This conformation might be caused by the KIF19A specific glycine mutation before the highly conserved RAK residues at the C-terminal end of the helix  $\alpha$ 6. Since the helix  $\alpha$ 6 serves as the base of the following neck-linker region that is necessary for the MT-based plus-end motility as well as the inter-head communication in case of the dimeric motility, this glycine mutation and short form of  $\alpha$ 6 might produce either positive or negative effect in the motility and the inter-head communication of KIF19A. Further structural and biochemical studies are needed to elucidate the functional role of the L8- $\alpha$ 3-L9 and the short helix  $\alpha$ 6.

### **Structural Mechanisms of Dual Functions of KIF19A.**

To achieve the dual functions of KIF19A, the MT-based motility and the MT-depolymerization, KIF19A needs to bind tightly both to two distinct interface, the straight tubulin-dimer on the MT-lattice and the helically curved tubulin-dimer at the MT-end (Figure 13). Previously reported motile kinesins only bind tightly to the former one, whereas depolymerizing kinesins (Kinesin-13s) only bind tightly to the latter one. KIF19A may accomplish this demanding task by the increasing flexibility of the MT-binding interface of KIF19A as well as introducing the long loop L2 like the MT-depolymerizing Kinesin-13s. MT-binding interface consists of following elements from the plus-end to the minus-end: the loop L8, the switch II cluster (L11- $\alpha$ 4-L12- $\alpha$ 5), the helix  $\alpha$ 6, and the loop L2. Among them, most prominent conformational change was observed at the switch II cluster of KIF19A. The helix  $\alpha$ 4 is atypically distantly positioned from the catalytic core (Figure 5). The protruding  $\alpha$ 4 was found for the first time among all the solved crystal structures of kinesins. At the ends of the helix  $\alpha$ 4, the loops L11 and L12 are destabilized and become flexible so that KIF19A might be able to adjust the position of the helix  $\alpha$ 4 to fit the two distinct binding partner, the straight tubulin-dimer and the curved tubulin-dimer.

Then, why the flexible positioning of the helix  $\alpha 4$  occurs specifically in KIF19A? When superimpose the KIF19A structure onto other kinesins, I found that about one turn melted at the N-terminal end of the helix  $\alpha 5$  (Figure 6). At that point, the highly conserved proline residue among all KIFs except for KIF19A is replaced with the unique asparagine residue (N297). In general, proline residue is often found at the starting or the ending points of the helix to stabilize it. In KIFs except for KIF19A, highly conserved proline is found at the starting point of the helix  $\alpha 5$  to stabilize it. Thus, the replacement of proline to the asparagine residue might destabilize  $\alpha 5$  to be melted into the flexible long loop L12. Therefore, I expected that the flexible positioning of the helix  $\alpha 4$  is caused by the KIF19A specific N297.

This idea was confirmed by the biochemical and biophysical experiments. N297P mutant presented about 30% increase of MT-stimulated ATPase activity and more than 30% decrease of the tubulin-stimulated ATPase activity in comparison with the wild type (Figure 9A,C). As a result, N297P mutation moved MTs 40% faster than the wild type (Figure 11D), whereas N297P mutant decrease the MT depolymerizing activity (Figure 12A). This indicates that N297P mutant, which fits better to the MT than to the curved-tubulin dimer

has the advantage for the MT-based motility. In other words, the KIF19A-specific asparagine residue becomes a key determinant to accommodate the KIF19A interface more to the curved tubulins so that KIF19A has acquired the higher depolymerizing activity at the expense of the motility speed.

Finally I discuss about the functional role of the loop L2. Both Kinesin-8 and Kinesin-13, the depolymerizing kinesins, are known to have an extended loop L2 comparing with other motile kinesins, albeit different depolymerizing efficiency. KIF19A and KIF2C have a comparable length of loop L2 (Figure 7C). Kinesin-13 has a class-specific lysine-valine-aspartate (KVD) finger structure that lies in the tip of loop L2 and any residue deletion of the KVD finger will deprive of the effective MT depolymerizing activity (Ogawa et al. 2004; Shipley et al. 2004). Interestingly, the loop L2 in the crystal structure of KIF19A is built up from a hydrophobic tip (I54, L55) sandwiched by the acidic (E49, D50, D52, D53) and basic clusters (R56, H58, R59, R61). The similar order of residue characters (basic-hydrophobic-acidic) in the loop L2 of KIF19A and KIF2C highlight the potential significance of the charged and hydrophobic residues in depolymerizing the MTs. The alanine mutations in each section, in fact, caused the MT depolymerizing deficiency (Figure

12). The same subclass Kinesin-8, KIF18A has the 9 residues longer than KIF19A, the charged residues seem to arrange randomly in the loop L2 of KIF18A, resulting in decreasing its depolymerizing activity (Figure 6C). What is more, the slender loop L2 (Figure 7D) and relatively longer antiparallel  $\beta$ -sheet of Kinesin-13 form more rigid protrusion that points down to the MT, just like a sharp dagger, resulting effective depolymerase activity. The long, fan-shaped loop L2 of KIF19A (Figure 7E) provides the possibility of flexible conformation, leading to a relatively low MT depolymerizing efficiency of the Kinesin-8.

In addition to the role for MT-depolymerization, the basic cluster of L2 of KIF19A also contributes to the processivity of KIF19A when moving along the MTs. PC2A mutants severely weakened the MT-binding affinity of KIF19A so that MT could not glide on the KIF19A clusters on the cover slide. The deletion of E-hook at the C-terminus of tubulins also has the same effect as the PC2A mutation, suggesting that KIF19A might tether the MT using the flexible ionic interaction between the positive charged residues of L2 of KIF19A and the E-hook of tubulins, similar with the interaction between the K-loop of KIF1A and E-hook of tubulins. As described above, KIF19A specific N297 has disadvantage for the

MT-based motility. Basic cluster might compensate this disadvantage by increasing the affinity of KIF19A to the MTs.

In summary, this study illustrates the functional anatomy for the dual function of KIF19A (Figure 13). Basic cluster of the loop L2 of KIF19A enables it to tether MTs by the flexible ionic interaction with the E-hook of tubulins so that KIF19A processively walks along the MT-lattice. When KIF19A reaches the plus-end of the MTs, the specific asparagine residue 297 of KIF19A as well as the flexible loop L8 facilitates the binding to the curved protofilament and then, the tubulin dimer is removed from the plus end of MTs by using the energy generated from ATP hydrolysis. The hydrophobic tip of L2 plays the critical role during the some step(s) of the depolymerization process. Therefore, KIF19A has acquired the dual function by introducing the multiple strategies, one of which resembles the KIF1A tethering to the MTs, the other of which resembles the Kinesin13s depolymerizing strategy. Further structural studies including the X-ray crystallography of KIF19A in another nucleotide state and the cryo-EM analysis of KIF19A-MT complex as well as the biochemical and cell biological studies are needed to clarify the full biological mechanism of the dual functions of KIF19A.

## Figure Legends

### Figure 1. Kinesin Superfamily Proteins

Phylogenetic classification of all the kinesin superfamily proteins (KIFs) expressed in mouse/ human, *D.melanogaster*, *C. elegans*, and *S.cerevisiae*. Modified with the author's permission (Miki et al. 2001; Miki et al. 2005). The red rectangle indicated the KIF19A motor protein.

### Figure 2. KIF19A motor domain construct and sequence alignment

(A) Schematic of Mouse KIF19A motor domain.

Top, Full length of KIF19A protein, the motor domain of KIF19A is colored in blue, followed by neck linker and short neck domain colored in black and magenta respectively, stalk and tail domain colored in orange.

Bottom, KIF19A-353WT, the construct used in this study is depicted in blue and followed by a 7XHis tag at the C terminus.

(B) Sequence Alignment of KIF19A, KIF18A, KIF2C, KIF5C and KIF1A.

Conserved residues are highlighted by black and grey. Structural elements, according to

standard nomenclature, are labeled on the top of alignment. The disordered parts of the structure are shown in dash lines.  $\beta$ 1b-L2- $\beta$ 1c,  $\beta$ 5a-L8- $\beta$ 5b- $\alpha$ 3, L11- $\alpha$ 4-L12, and  $\alpha$ 6 are colored in yellow, green, magenta and light blue respectively. Negative charged and positive charged residues in L2 of KIF19A and KIF2C are indicated in red and blue. One of KIF19A specific residues, N297, is colored in purple.

**Figure 3. Purification, crystallization and data collection of KIF19A353WT**

- (A) A chromatogram of cation exchange chromatography (Resource S)
- (B) SDS-PAGE image of purification sampling. The molecular markers are in the left lane. Sup: supernatant, FL: flow through, W: wash, D1/D2: Dialysis1/2.P1/P2/P3: Peak1/2/3 in (A). The red rectangle indicated the pooled fractions used for concentration and crystallization.
- (C) Crystal examples of KIF19A353WT, scale bar 0.1 mm.
- (D) X-ray diffraction image of KIF19A353WT. The dash line indicates the resolution limit.

#### **Figure 4. S-SAD guided model building**

The difference map ( $\sigma=\pm 2.5$ ) calculated with preliminary model illustrates the unusual helical density close to the loop L2. The dash line rectangle showed the under-determination helix. The anomalous difference Fourier map clearly shows the diffraction from the sulfur atoms and the phosphorus atoms.

(B) Met248, (C) ADP, and (D) Cys283. The sulfur atom in methionine and cysteine residues are colored in yellow. The phosphorus atom in ADP are colored in orange.

#### **Figure 5. Overall architecture of KIF19A motor domain.**

KIF19A motor domain is seen from the MT binding side (A) and the opposite side(C).

(B) Rotate the model (A) 90° around axis of ordinate. The color pattern is same with

Figure 2B. Mg<sup>2+</sup>ADP is shown as a ball and stick model.

#### **Figure 6. Structural comparison of KIF19A and KIF18A motor domain**

(A) Superposition of KIF19A353WT and KIF18A motor domain (KIF18A-ADP, PDB

ID code is 3LRE) and 90°-rotation model (B). The different structural elements were

colored in red (KIF19A) and green (KIF18A). KIF19A specific residue Asn297 and the counterpart of KIF18A Pro307 are highlighted in sphere model. Sequence alignment of MmKIF19 and MmKIF18A within  $\beta$ 1b-L2- $\beta$ 1c (C),  $\alpha$ 6 (D), and L11- $\alpha$ 4-L12 (E).

### **Figure 7. Structural comparison of KIF19A and KIF2C motor domain**

(A) Superposition of KIF19A353WT and KIF2C motor domain (KIF12C-ADP, PDB ID code is 1V8J) and 90°-rotation model (B). The different structural elements were colored in red (KIF19A) and gold (KIF2C).

(C) Loop L2 Sequence alignment of MmKIF19 and MmKIF2C.

Loop L2 structure of KIF2C (D) and KIF19A (E) are shown separately.

### **Figure 8. Structural comparison of KIF19A, KIF1A and KIF4 motor domain**

(A) Superposition of KIF19A353WT and KIF1A motor domain (KIF1A-ADP, PDB ID code is 2ZFI). The different structural elements were colored in red (KIF19A) and light blue (KIF1A).

(B) Superposition of KIF19A353WT and KIF4 motor domain (KIF4-AMPPNP, PDB

ID code is 3ZFC). The different structural elements were colored in red (KIF19A) and blue (KIF4).

(C) 12° counter clockwise rotation of L8- $\alpha$ 3-L9 cluster of KIF19A might close the nucleotide-binding pocket. The high transparent model indicated the original position before rotation.

### **Figure 9. Steady state ATPase kinetics of KIF19A353WT and its mutants**

(A) The basal ATPase activity of KIF19A353WT and its mutants

(B) MT-stimulated ATPase activity of KIF19A353WT and its mutants

(C) Tubulin-stimulated ATPase activity of KIF19A353WT and its mutants

(D) Michaelis-Menten kinetics of  $k_{cat}$  comparison between the of KIF19A353WT and its mutants

(E) Michaelis constant  $K_M$  comparison between the of KIF19A353WT and its mutants

All the data were from three independent experiments. Error bar represent the standard deviation (SD).

**Figure 10. L2 defect mutant decreases the binding affinity between KIF19A and**

**MTs**

(A) Binding curve of KIF19A in the AMPPNP state for MTs. The binding fraction plotted against the concentration of polymerized tubulins (MTs). The dissociation constant values were listed in the table below the curve. All the data were from three independent experiments. Error bars represent the standard deviation (SD).

(B) Different concentration of KIF19A motor domain binds to MT polymerized by tubulin or tubulins S.

**Figure 11. MT glides faster on mutants N297P than KIF19A353WT**

(A) Schematic of flow chamber used in this study. Arrows showing the solution flow direction.

(B) Schematic representation of *in vitro* gliding assay depicting KIF19A protein (light blue) immobilized on the glass glide by penta His antibody (blue). MT (red) can glide on the motor protein KIF19A.

(C) Representative kymographs showing KIF19A353WT and mutant N297P gliding

track.

(D) Motility velocity Diagram of KIF19A353WT (n=167) and mutant N297P (n=110)

### **Figure 12. Depolymerization activities of KIF19A353WT and its mutants**

(A) GMPCPP-stabilized MTs was incubated with KIF19A353WT or its mutants in the presence of MgATP for at 25°C. Soluble tubulin (S) and the remaining MTs in the pellets (P) were separated by centrifuge and analyzed by SDS-PAGE followed by Coomassie Bright Blue staining.

(B) Depolymerization curve of KIF19A353WT and its mutants.

All the data were from three independent experiments. Error bars represent the standard deviation (SD).

### **Figure 13. KIF19A Dual Functional Model**

(A) The ATP hydrolysis cycles during MT lattice-based motility and MT plus-end depolymerization of KIF19A.

(B) The complex structure of KIF19A and two kinds of tubulin dimer, the straight and

curved tubulin.

(C) Binding of MTs may induce the structural changes of KIF19A motor domain.

Figure 1

The Kinesin Superfamily Proteins (KIFs)

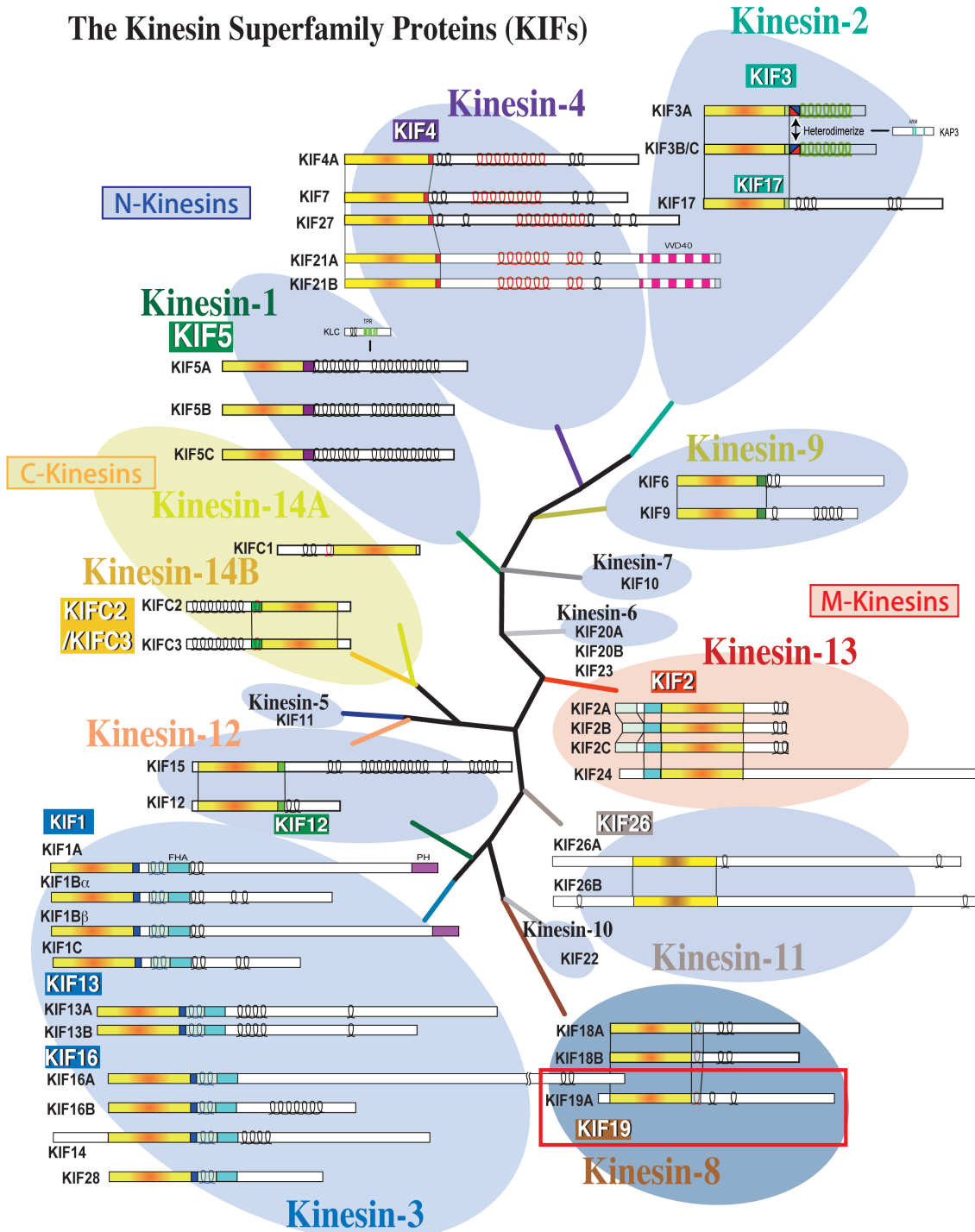




Figure 3

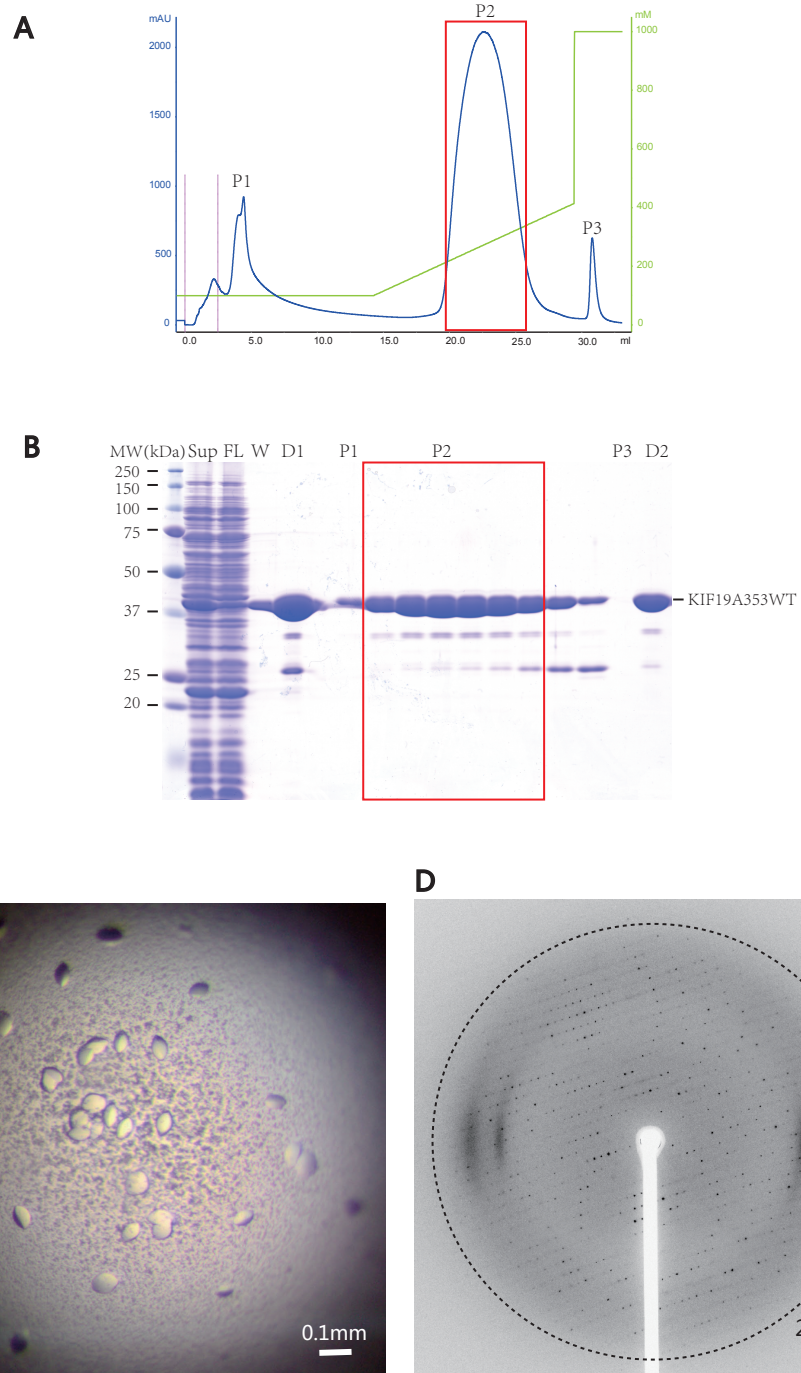


Figure 4

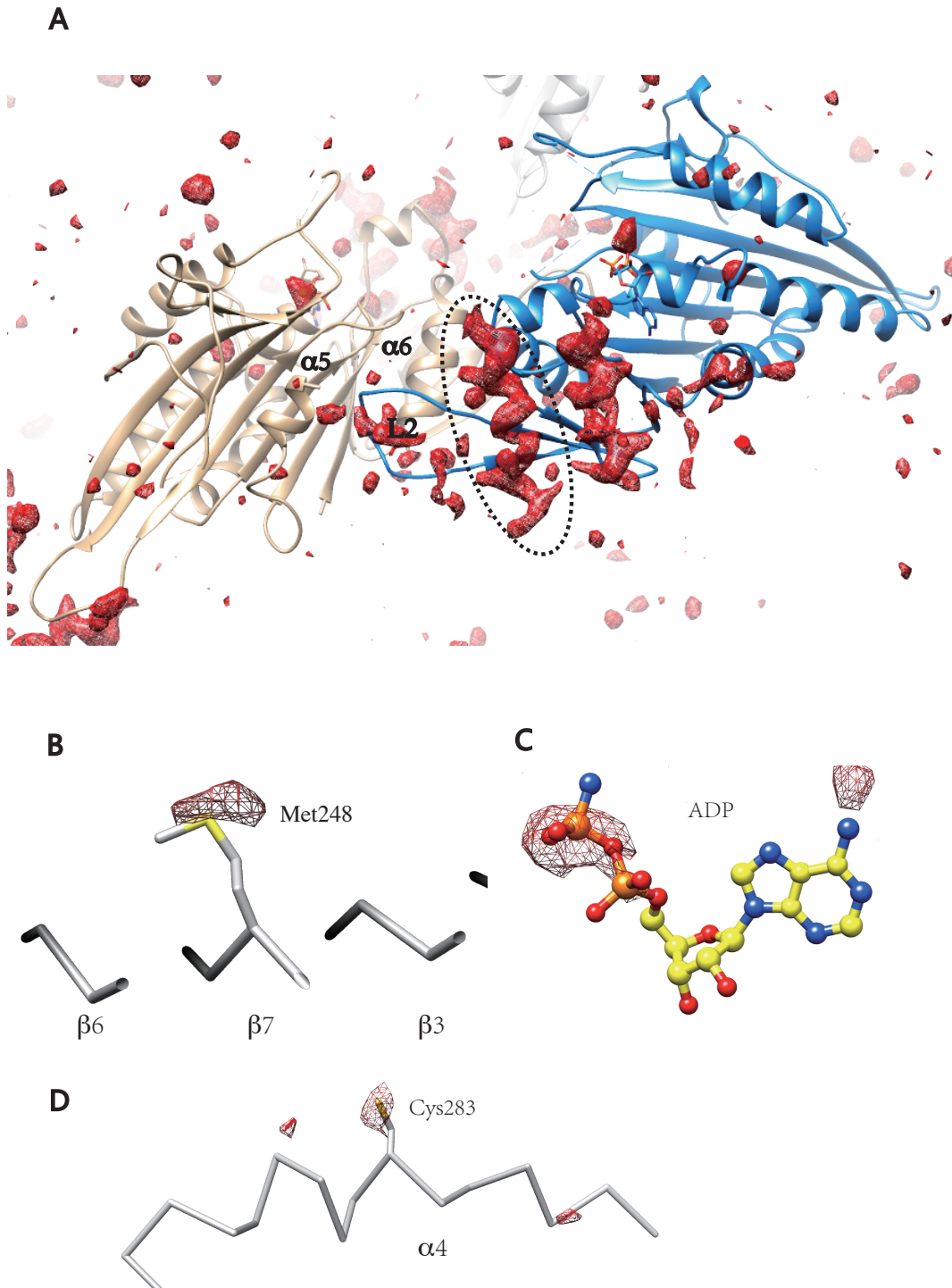


Figure 5

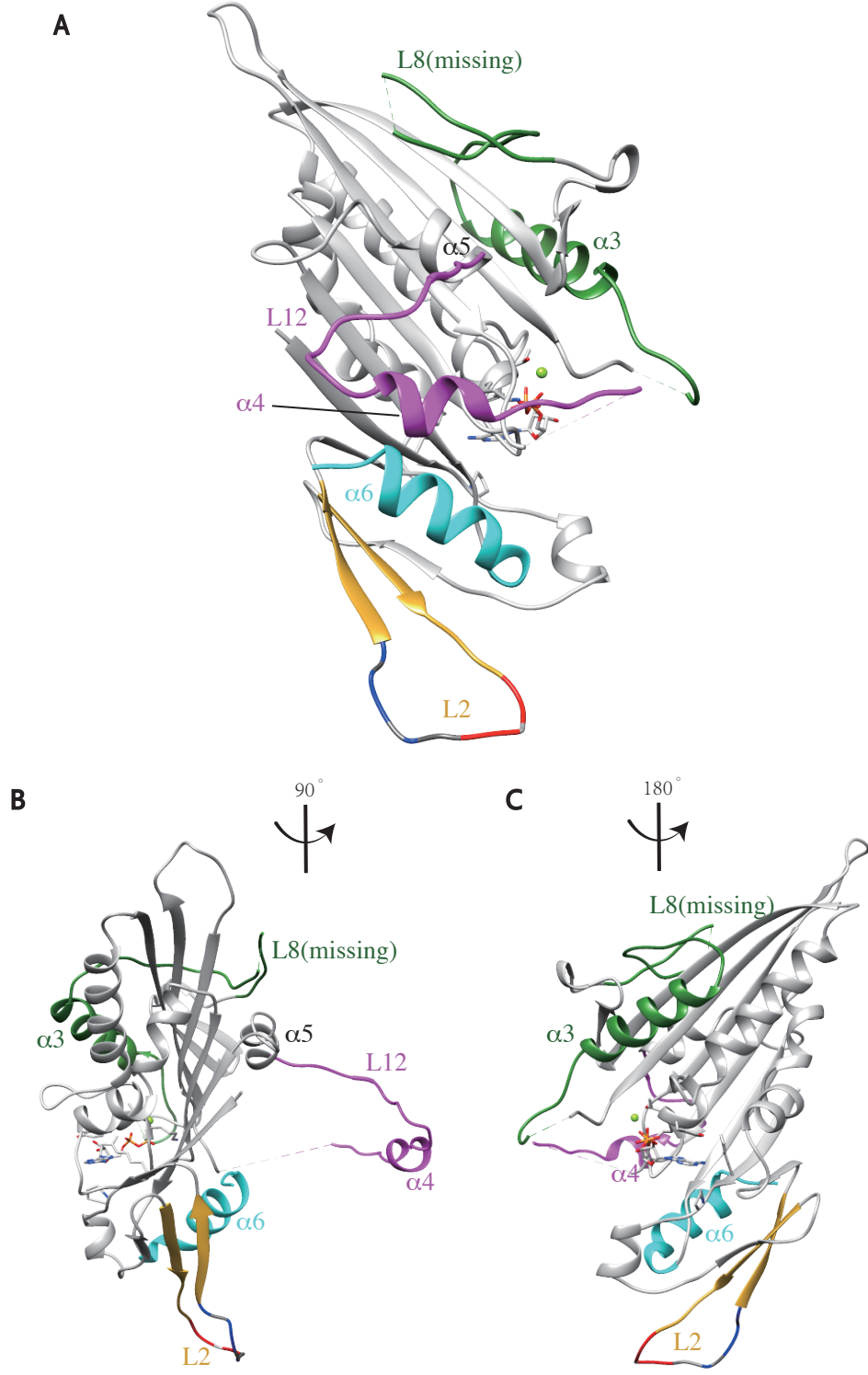


Figure 6

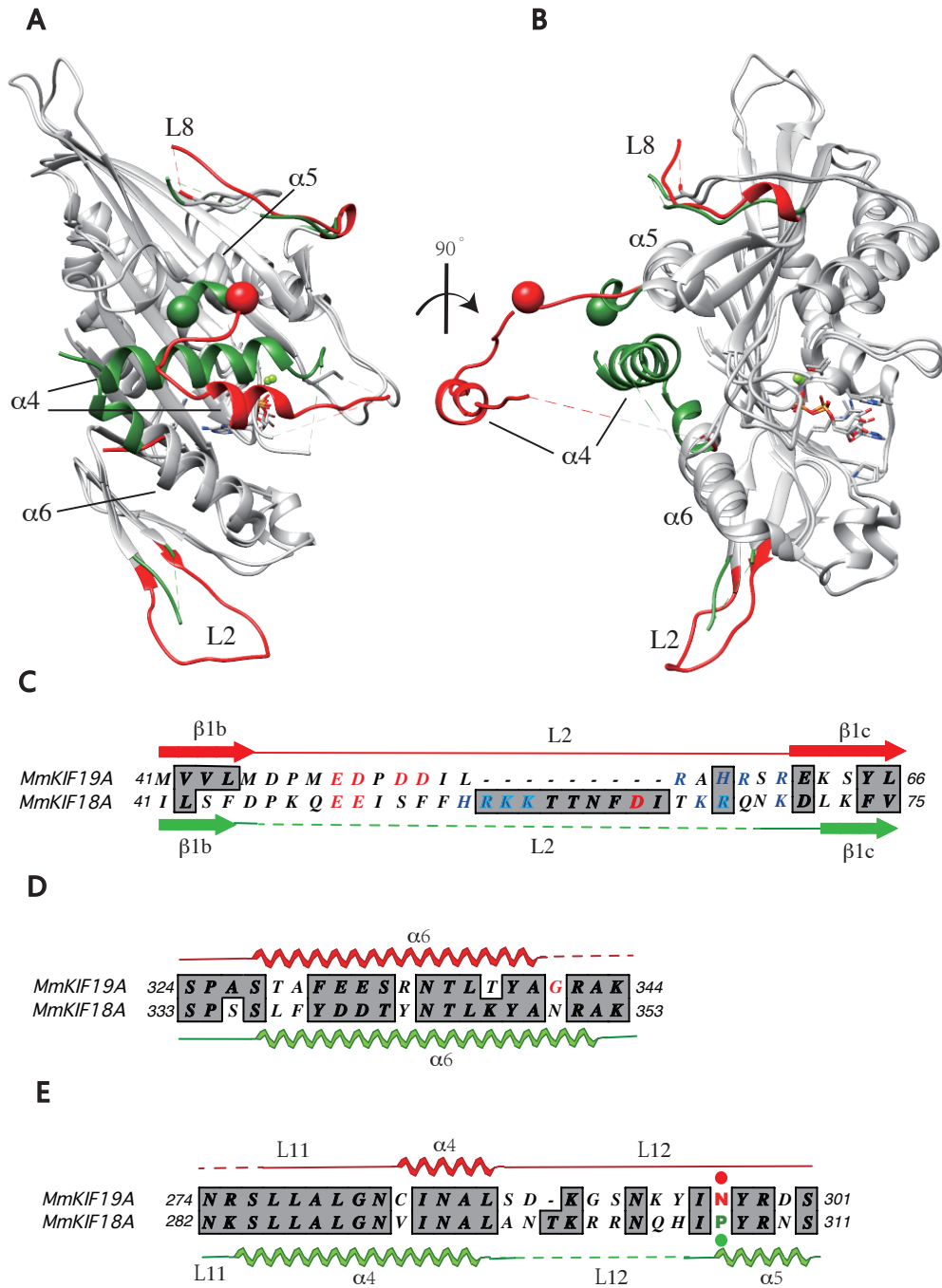


Figure 7

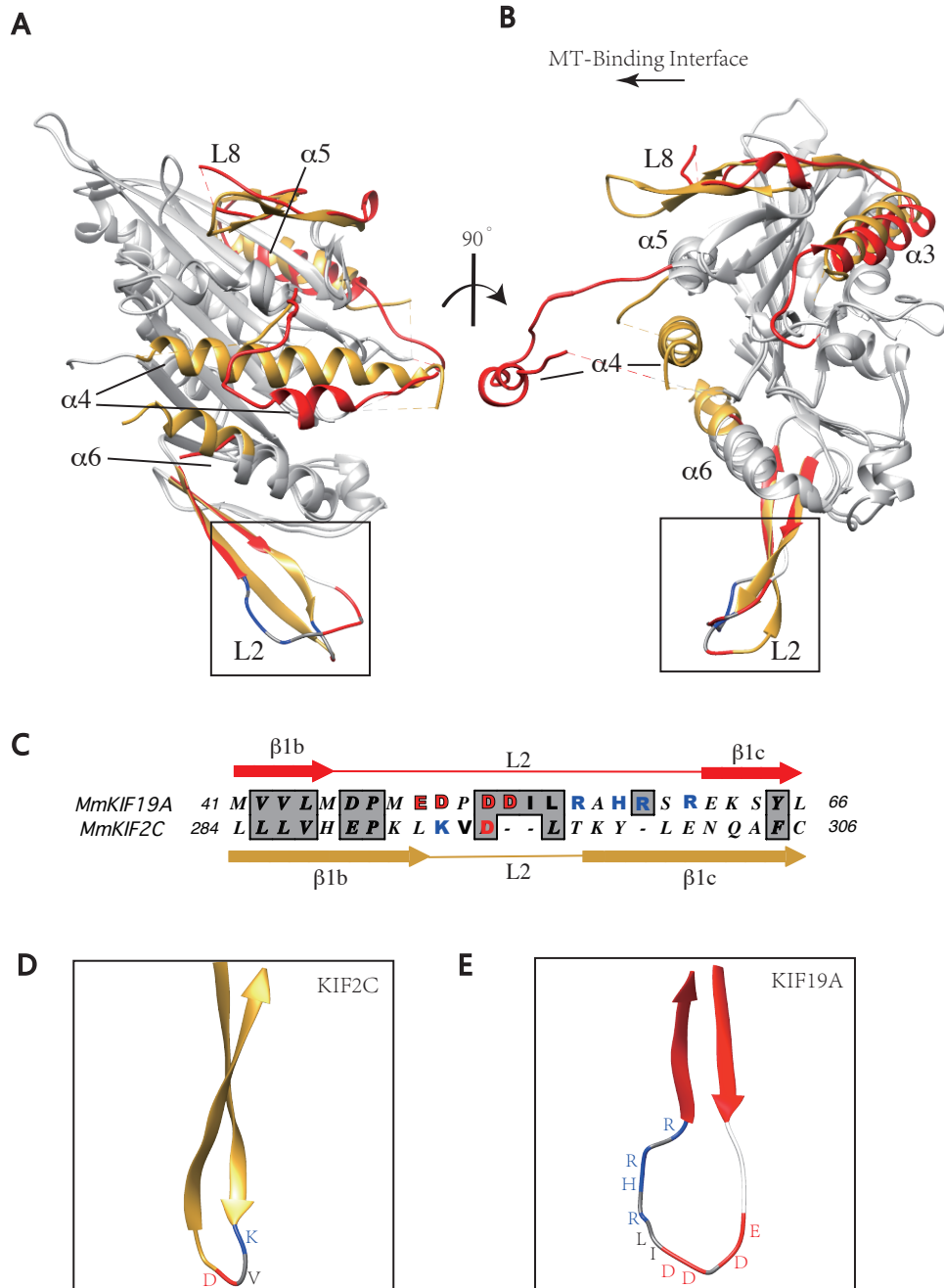


Figure 8

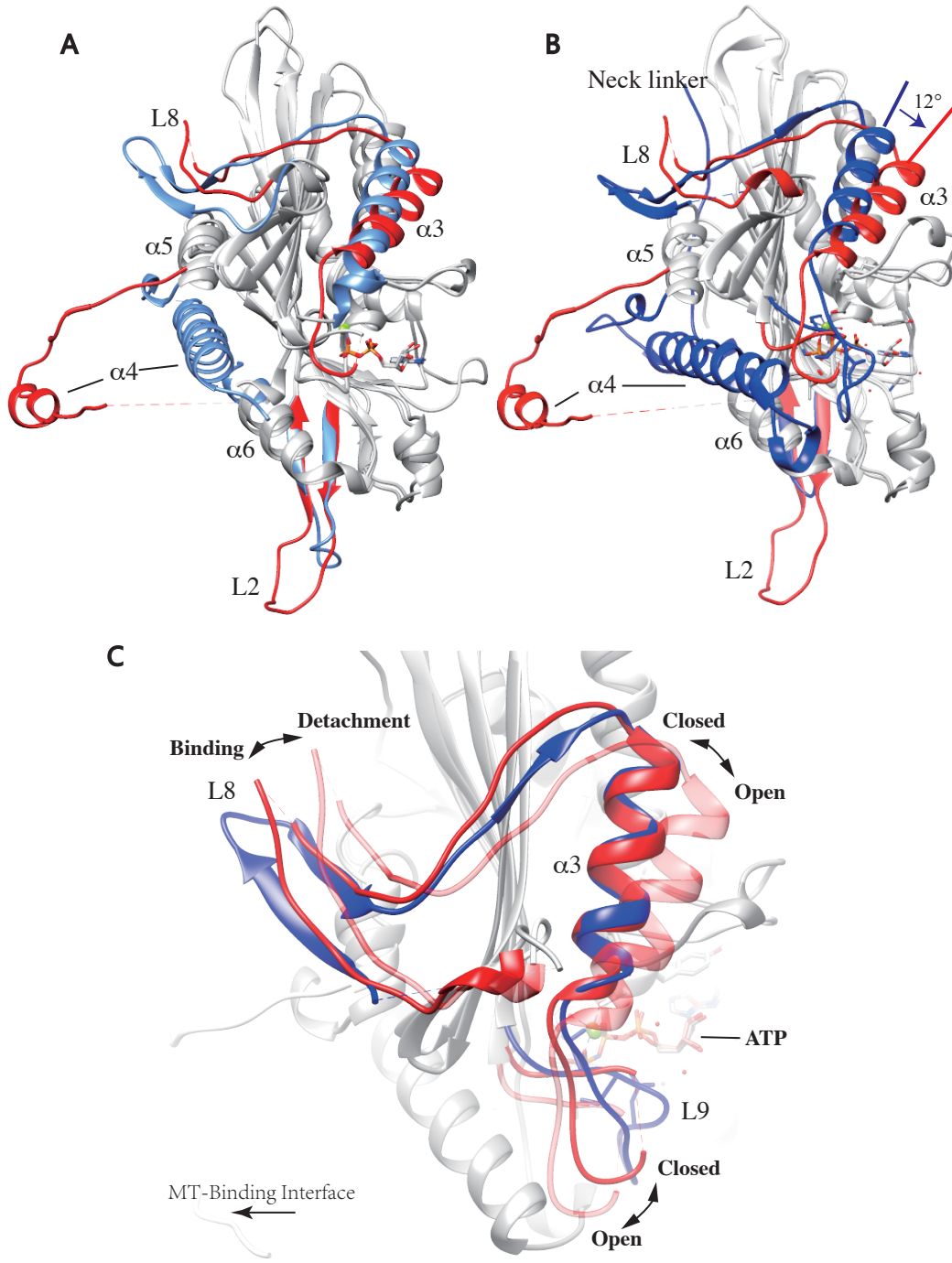


Figure 9

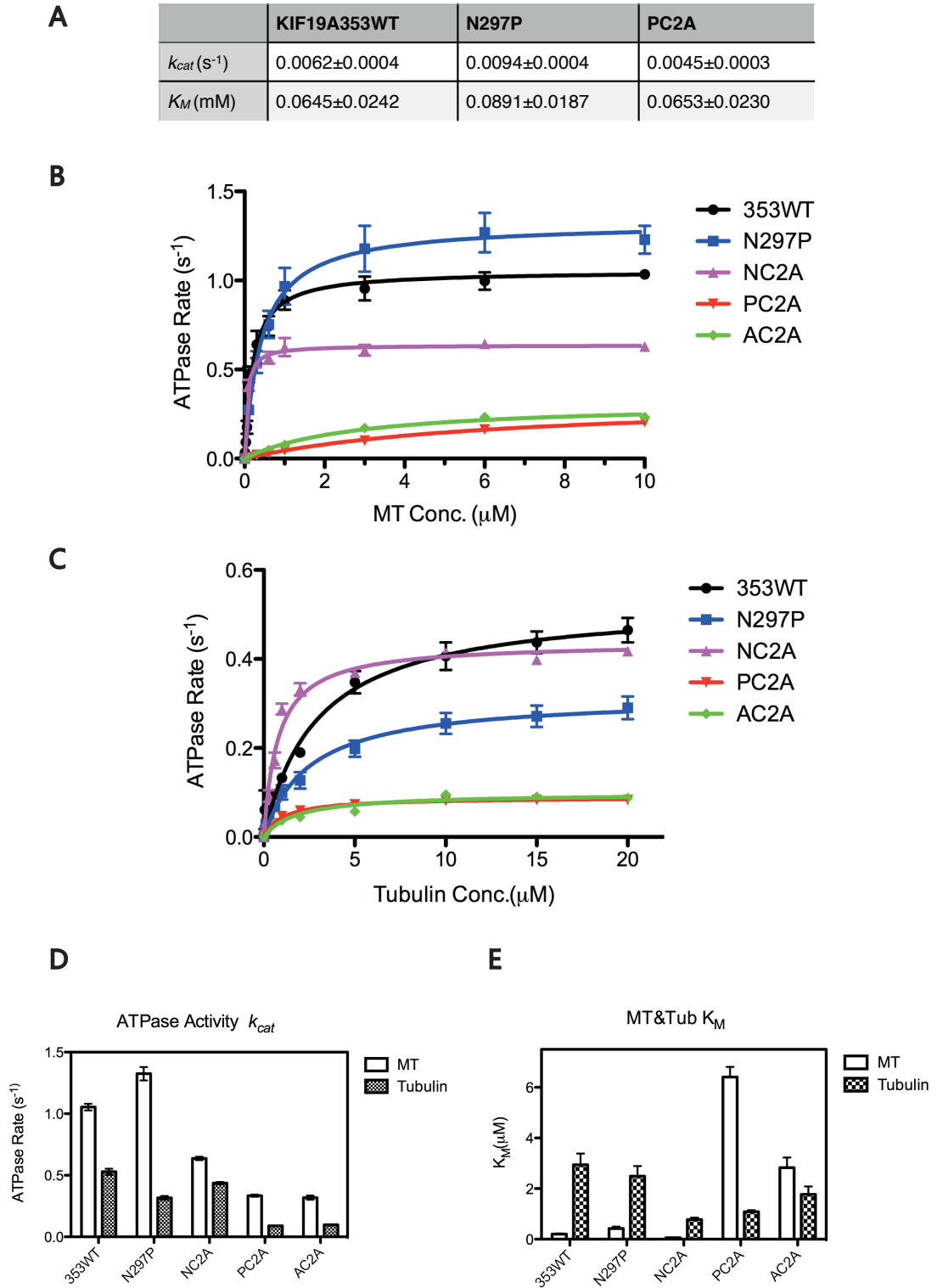
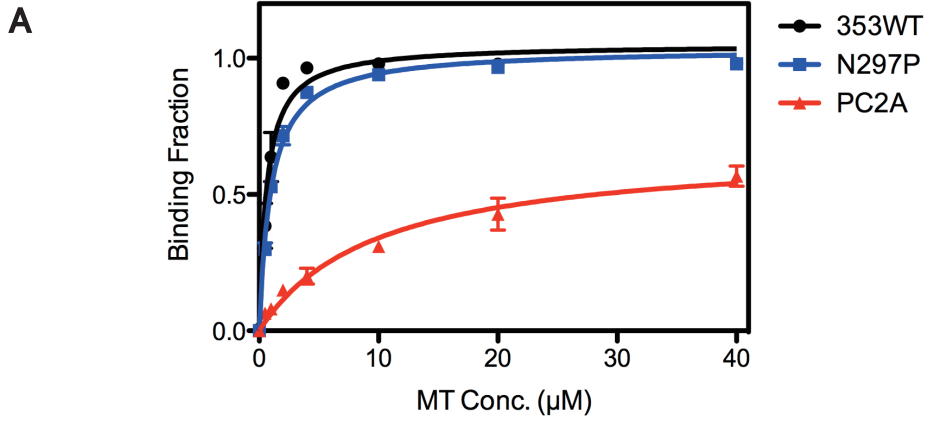


Figure 10



	KIF9A353WT	N297P	PC2A
<b>Bmax</b>	1.047±0.031	1.031±0.015	0.673±0.052
<b>Kd(µM)</b>	0.6140±0.099	0.9681±0.067	9.745±2.034

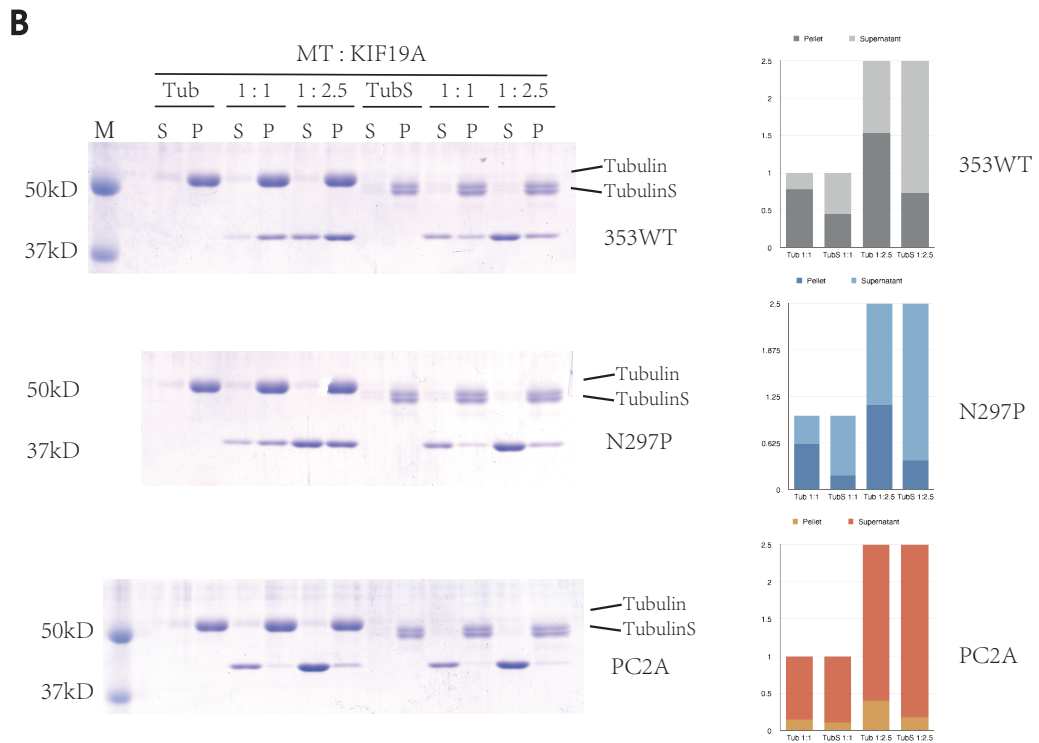


Figure 11

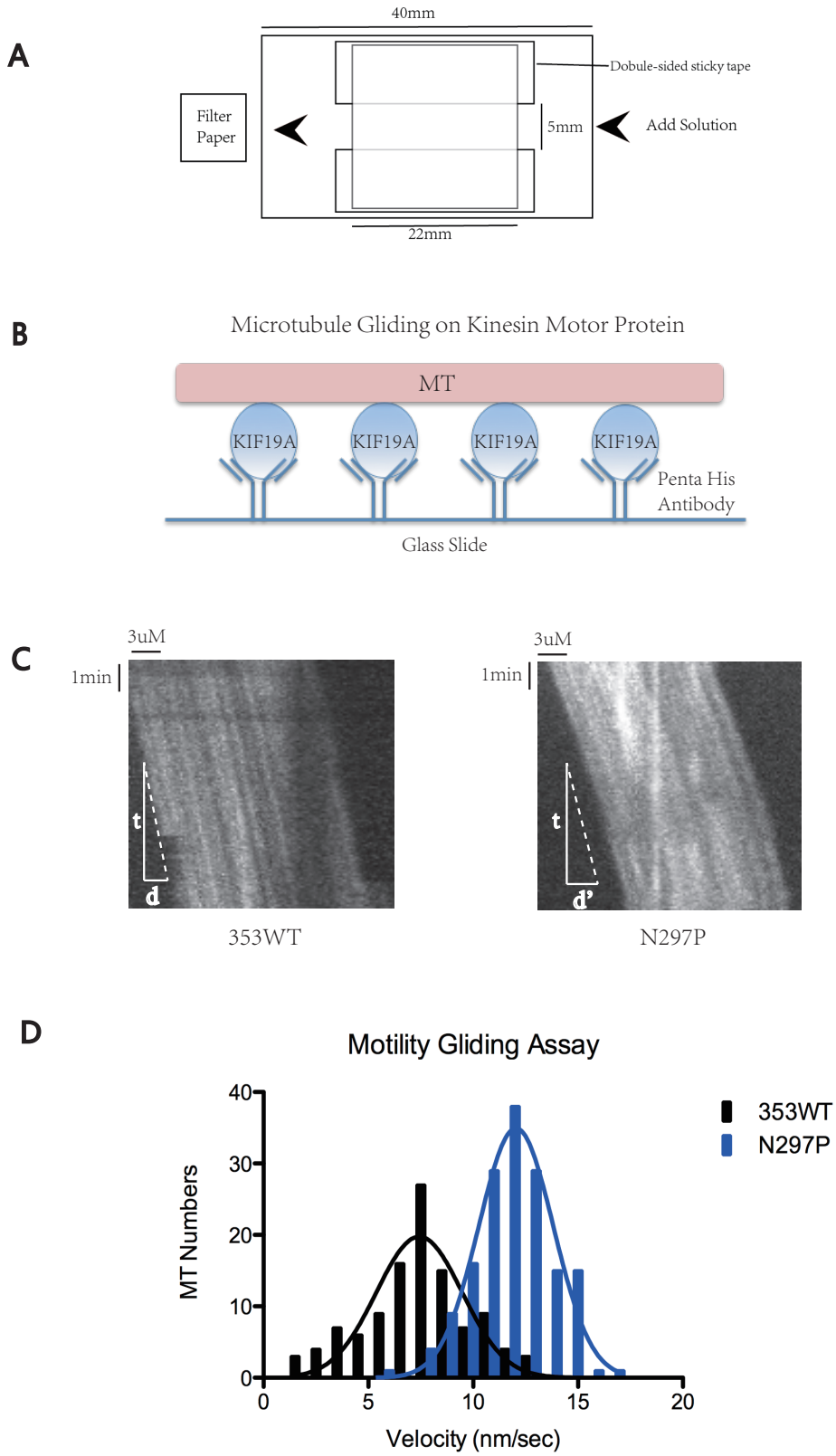


Figure 12

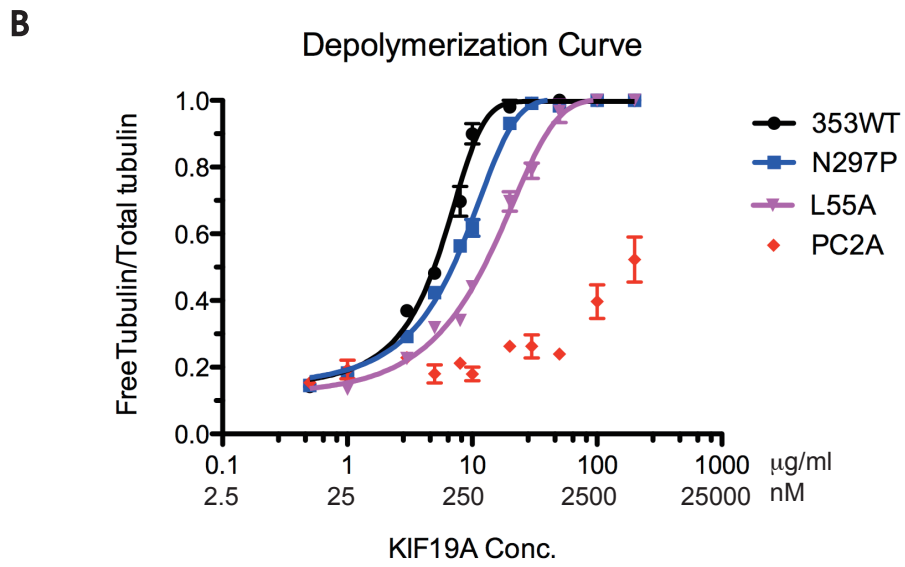
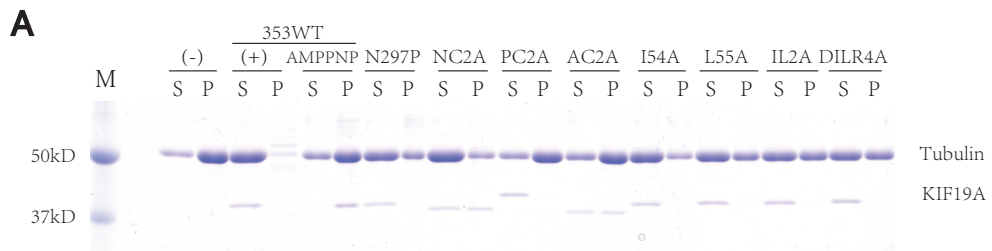


Figure 13

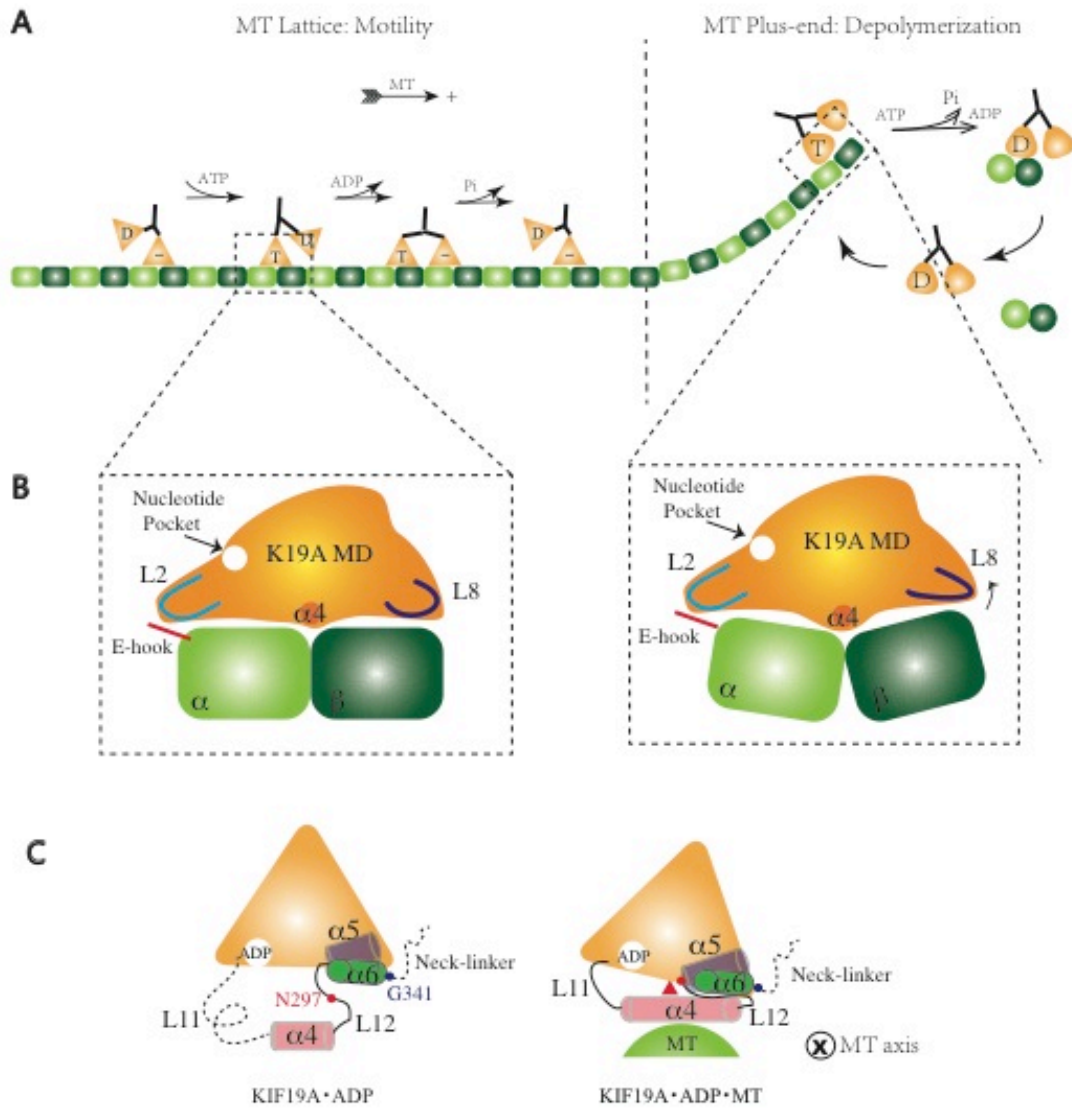


Table 1. The primer information of KIF19A constructs

<b>Primer</b>	<b>Sequence</b>
<b>KIF19A353WT_Forward</b>	CCCGGAATTCCATGAAGGACAGCGGTGACTC
<b>KIF19A353WT_Reverse</b>	GACGTCGACCTAATGGTGATGGTGATGGTGATGGTTCTGCTTCACCCGAGTCC
<b>N297P_Forward</b>	AGGGCAGTAATAAATACATCCCCTATCGGGACAGCAAACCTC
<b>N297P_Reverse</b>	GAGTTTGCTGTCCCGATAGGGGATGTATTTATTACTGCCCT
<b>NC2A_Forward</b>	CGGCCCTGCCGCCATTCTGCGGGCACACCGGTCCCGG
<b>NC2A_Reverse</b>	GCGGCAGGCCCCGCCATTGGGTCCATGAGAACCACCAT
<b>PC2A_Forward</b>	GCGGCAGCCGCGTCCGCGGAGAAGTCATACCTCTTTGACGTG
<b>PC2A_Reverse</b>	GCGGACGCGGCTGCCGCCAGAATGTCGTCAGGGTCTCCAT
<b>AC2A_Forward</b>	ATGGCGGCCCTGCCGCCATTCTGGCGGCAGGGGCCGCCAT
<b>AC2A_Reverse</b>	CTCCGCGGACGCGGCTGCCGCCAGAATGGCGGCAGGGGCCGCCAT
<b>I54A_Forward</b>	GAGGACCCTGACGACGCTCTGCGGGCACACCG
<b>I54A_Reverse</b>	CGGTGTGCCCCGAGAGCGTCGTCAGGGTCCTC
<b>L55A_Forward</b>	GACCCTGACGACATTGCGCGGGCACACCGGTC
<b>L55A_Reverse</b>	GACCGGTGTGCCCGCAATGTCGTCAGGGTC
<b>IL2A_Forward</b>	GAGGACCCTGACGACGCTGCGCGGGCACACCGGTC
<b>IL2A_Reverse</b>	GACCGGTGTGCCCGCAGCGTCGTCAGGGTCCTC
<b>DILR4A_Forward</b>	TGGAGGACCCTGACGCCGCTGCGGCGGCACACCGGTCCCG
<b>DILR4A_Reverse</b>	CGGGACCGGTGTGCCCGCCGAGCGGCGTCAGGGTCCTCCA

Table 2. Buffer Information

<b>Buffers</b>	<b>Components</b>
<b>Lysis Buffer</b>	50mM Tris-HCl (pH 8.0), 500mM NaCl, 5mM Imidazole
<b>Wash Buffer</b>	50mM Tris-HCl (pH 8.0), 500mM NaCl, 50mM Imidazole
<b>Elution Buffer</b>	50mM Tris-HCl (pH 8.0), 500mM NaCl, 500mM Imidazole
<b>CIEX Buffer B1</b>	100mM Mes (pH 6.0), 1mM MgCl <sub>2</sub> , 15% Sucrose
<b>CIEX Buffer B2</b>	100mM Mes (pH 6.0), 1mM MgCl <sub>2</sub> , 1M NaCl, 15% Sucrose
<b>Dialysis Buffer1</b>	10mM MOPS (pH 7.0), 1mM MgCl <sub>2</sub> , 100nM NaCl, 15% Sucrose, 1mM DTT, 1mM EGTA, 0.1 mM ADP
<b>Dialysis Buffer2</b>	10mM MOPS (pH 7.0), 1mM MgCl <sub>2</sub> , 100nM NaCl, 15% Sucrose, 0.1 mM ADP
<b>BRB80</b>	80mM PIPES (pH 6.9, KOH), 1mM EGTA, 1mM MgCl <sub>2</sub>
<b>PEM</b>	100mM PIPES (pH 6.9, KOH), 1mM EGTA, 1mM MgCl <sub>2</sub>
<b>Oxygen-Scavenger</b>	45 mg/ml Glucose, 0.05 mg/ml Catalase, 0.05 mg/ml Glucose oxidase, 2mM Phosphoenolpyruvic acid (PEP), 0.1 mg/ml Pyruvate Kinase (PK)

**Table 3. Data collection and refinement statistics**

KIF19A353WT	
<b>Data collection</b>	
Space group	P4 <sub>2</sub> 2 <sub>1</sub> 2
Cell dimensions	
<i>a, b, c</i> (Å)	122.604, 122.604, 56.198
$\alpha, \beta, \gamma$ (°)	90, 90, 90
Resolution (Å)	2.718
<i>R</i> <sub>sym</sub> or <i>R</i> <sub>merge</sub>	0.132
<i>I</i> / $\sigma I$	34.7
Completeness (%)	99.8
Redundancy	13.6
<b>Refinement</b>	
Resolution (Å)	47.16-2.72
No. reflections	11438
<i>R</i> <sub>work</sub> / <i>R</i> <sub>free</sub>	24.53% / 30.06%
No. atoms	
Protein	2256
Ligand/ion	29
Water	183
R.m.s. deviations	
Bond lengths (Å)	0.0125
Bond angles (°)	1.7055

## References

- Brunger, A.T., 2007. Version 1.2 of the Crystallography and NMR system. *Nature Protocols*, 2(11), pp.2728–2733.
- Brunger, A.T. et al., 1998. Crystallography & NMR system: A new software suite for macromolecular structure determination. *Acta Crystallographica Section D Biological Crystallography*, 54(5), pp.905–921.
- Case, R.B. et al., 2000. Role of the kinesin neck linker and catalytic core in microtubule-based motility. *Current biology : CB*, 10(3), pp.157–160.
- Dauter, Z. et al., 1999. Can anomalous signal of sulfur become a tool for solving protein crystal structures? *Journal of molecular biology*, 289(1), pp.83–92.
- Desai, A. et al., 1999. Kin I kinesins are microtubule-destabilizing enzymes. *Cell*, 96(1), pp.69–78.
- Emsley, P. & Cowtan, K., 2004. research papers. *Acta Cryst (2004). D60, 2126-2132 [doi:10.1107/S09074444904019158]*, pp.1–7.
- Gell, C. et al., 2010. Microtubule Dynamics Reconstituted In Vitro and Imaged by Single-Molecule Fluorescence Microscopy. In *Methods in cell .... Methods in Cell Biology*. Elsevier, pp. 221–245.
- Gupta, M.L., Jr et al., 2006. Plus end-specific depolymerase activity of Kip3, a kinesin-8 protein, explains its role in positioning the yeast mitotic spindle. *Nature cell biology*, 8(9), pp.913–923.
- Helenius, J. et al., 2006. The depolymerizing kinesin MCAK uses lattice diffusion to rapidly target microtubule ends. *Nature cell biology*, 441(7089), pp.115–119.
- Hendrickson, W.A. & Teeter, M.M., 1981. Structure of the hydrophobic protein crambin determined directly from the anomalous scattering of sulphur.

- Hertzer, K.M. et al., 2006. Full-length dimeric MCAK is a more efficient microtubule depolymerase than minimal domain monomeric MCAK. *Molecular biology of the cell*, 17(2), pp.700–710.
- Hirokawa, N. et al., 2009. Kinesin superfamily motor proteins and intracellular transport. *Nature reviews Molecular cell biology*, 10(10), pp.682–696.
- Hunter, A.W. et al., 2003. The kinesin-related protein MCAK is a microtubule depolymerase that forms an ATP-hydrolyzing complex at microtubule ends. *Molecular cell*, 11(2), pp.445–457.
- Kikkawa, M., 2008. The role of microtubules in processive kinesin movement. *Trends in Cell Biology*, 18(3), pp.128–135.
- Kline-Smith, S.L. & Walczak, C.E., 2004. Mitotic spindle assembly and chromosome segregation: refocusing on microtubule dynamics. *Molecular cell*, 15(3), pp.317–327.
- Lawrence, C.J., 2004. A standardized kinesin nomenclature. *The Journal of cell biology*, 167(1), pp.19–22.
- Maney, T., 2001. Molecular Dissection of the Microtubule Depolymerizing Activity of Mitotic Centromere-associated Kinesin. *Journal of Biological Chemistry*, 276(37), pp.34753–34758.
- Mayr, M.I. et al., 2011. A Non-Motor Microtubule Binding Site Is Essential for the High Processivity and Mitotic Function of Kinesin-8 Kif18A D. Foltz, ed. *PLoS One*, 6(11), p.e27471.
- Mayr, M.I. et al., 2007. The Human Kinesin Kif18A Is a Motile Microtubule Depolymerase Essential for Chromosome Congression. *Current Biology*, 17(6), pp.488–498.
- Miki, H. et al., 2001. All kinesin superfamily protein, KIF, genes in mouse and human. *Proceedings of the National Academy of Sciences of the United States of America*, 98(13), pp.7004–7011.
- Miki, H., Okada, Y. & Hirokawa, N., 2005. Analysis of the kinesin superfamily: insights into structure and function. *Trends in Cell Biology*, 15(9), pp.467–476.

- Murshudov, G.N. et al., 2011. REFMAC5 for the refinement of macromolecular crystal structures. *Acta Cryst (2011)*. D67, 355-367 [doi:10.1107/S0907444911001314], pp.1–13.
- Nitta, R., Okada, Y. & Hirokawa, N., 2008. Structural model for strain-dependent microtubule activation of Mg-ADP release from kinesin. *Nature Structural & Molecular Biology*, 15(10), pp.1067–1075.
- Niwa, S. et al., 2012. KIF19A Is a Microtubule-Depolymerizing Kinesin for Ciliary Length Control. *Developmental cell*, 23(6), pp.1167–1175.
- Ogawa, T. et al., 2004. A common mechanism for microtubule destabilizers-M type kinesins stabilize curling of the protofilament using the class-specific neck and loops. *Cell*, 116(4), pp.591–602.
- Okada, Y. & Hirokawa, N., 2000. Mechanism of the single-headed processivity: diffusional anchoring between the K-loop of kinesin and the C terminus of tubulin. *Proceedings of the National Academy of Sciences of the United States of America*, 97(2), pp.640–645.
- Otwinowski, Z. & Minor, W., 1997. Processing of X-ray Diffraction Data Collected in Oscillation Mode. *Methods enzymol*, 276, pp.307–326.
- Peters, C. et al., 2010. Insight into the molecular mechanism of the multitasking kinesin-8 motor. *The EMBO Journal*, 29(20), pp.3437–3447.
- Pettersen, E.F. et al., 2004. UCSF Chimera?A visualization system for exploratory research and analysis. *Journal of Computational Chemistry*, 25(13), pp.1605–1612.
- Sack, S., Kull, F.J. & MANDELKOW, E., 1999. Motor proteins of the kinesin family. Structures, variations, and nucleotide binding sites. *European journal of biochemistry / FEBS*, 262(1), pp.1–11.
- Shipley, K. et al., 2004. Structure of a kinesin microtubule depolymerization machine. *The EMBO Journal*, 23(7).

- Stumpff, J. et al., 2011. A Tethering Mechanism Controls the Processivity and Kinetochores-Microtubule Plus-End Enrichment of the Kinesin-8 Kif18A. *Molecular cell*, 43(5), pp.764–775.
- Stumpff, J. et al., 2008. The Kinesin-8 Motor Kif18A Suppresses Kinetochores Movements to Control Mitotic Chromosome Alignment. *Developmental cell*, 14(2), pp.252–262.
- Su, X. et al., 2011. Mechanisms Underlying the Dual-Mode Regulation of Microtubule Dynamics by Kip3/Kinesin-8. *Molecular cell*, 43(5), pp.751–763.
- Su, X. et al., 2013. Microtubule-sliding activity of a kinesin-8 promotes spindle assembly and spindle-length control. *Nature cell biology*, 15(8), pp.948–957.
- Vale, R.D., 2003. The molecular motor toolbox for intracellular transport. *Cell*, 112(4), pp.467–480.
- Varga, V. et al., 2009. Kinesin-8 Motors Act Cooperatively to Mediate Length-Dependent Microtubule Depolymerization. *Cell*, 138(6), pp.1174–1183.
- Varga, V. et al., 2006. Yeast kinesin-8 depolymerizes microtubules in a length-dependent manner. *Nature cell biology*, 8(9), pp.957–962.
- Weaver, L.N. et al., 2011. Kif18A Uses a Microtubule Binding Site in the Tail for Plus-End Localization and Spindle Length Regulation. *Current biology : CB*, 21(17), pp.1500–1506.

## **Acknowledgements**

First and foremost, I would like to extend my sincere gratitude to Professor Nobutaka Hirokawa, for his kind support, encouragement and advices for completing the KIF19A project.

I really appreciate Dr. Ryo Nitta for his scientific supervision and instructive advices on the KIF19A project. I am deeply grateful of his help in completion of this thesis. My sincere thanks are also given to Drs. S. Inoue, T. Ogawa, H. Yajima, Ruyun Zhou, Wenxing Yang and Li Wang for their technical supports and discussions; Ms. Haruyo Fukuda and Hiromi Sato for their generous assistance and all other members of the Hirokawa laboratory for their suggestions.

Last but not least, my thanks would go to my beloved parents and friends for their loving considerations and great confidence in me all through four years. Special thanks are given to Zhidong Xu for his constant encouragement and support.